Biogeosciences

Supplement of

On the predictability of turbulent fluxes from land: PLUMBER2 MIP experimental description and preliminary results

Gab Abramowitz et al.

*Correspondence to:* Gab Abramowitz (gabriel@unsw.edu.au)
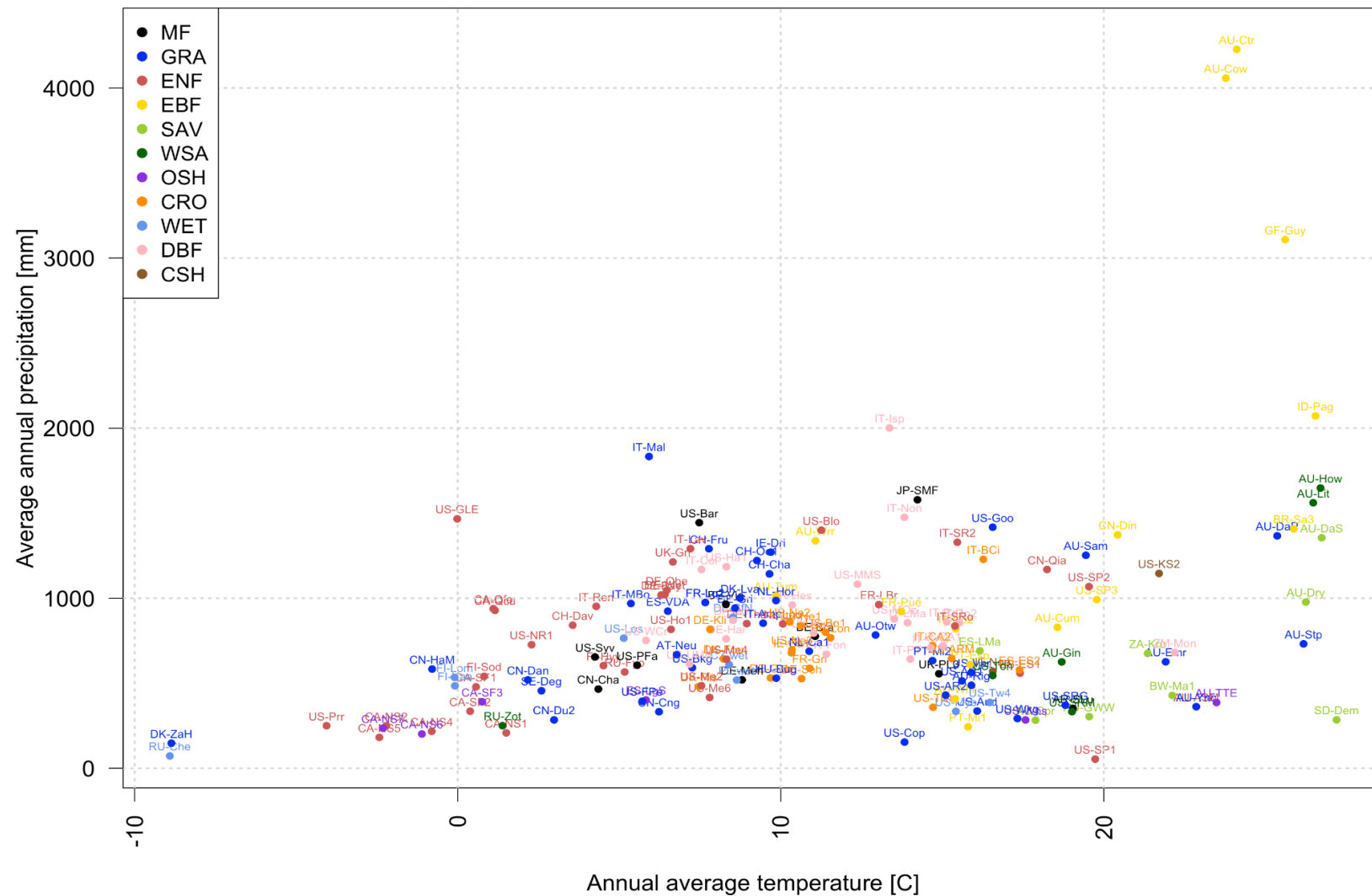
Figure S1: Distribution of site International Geosphere–Biosphere Programme vegetation types by Mean Annual Precipitation and Mean Annual Temperature. Vegetation types are: Mixed Forest (MF); Grassland (GRA); Evergreen Needleleaf (ENF); Evergreen Broadleaf (EBF); Savanna (SAV); Woody Savanna (WSA); Open Shrubland (OSH); Cropland (CRO); Wetland (WET); Deciduous Broadleaf (DBF); Closed Shrubland (CSH).
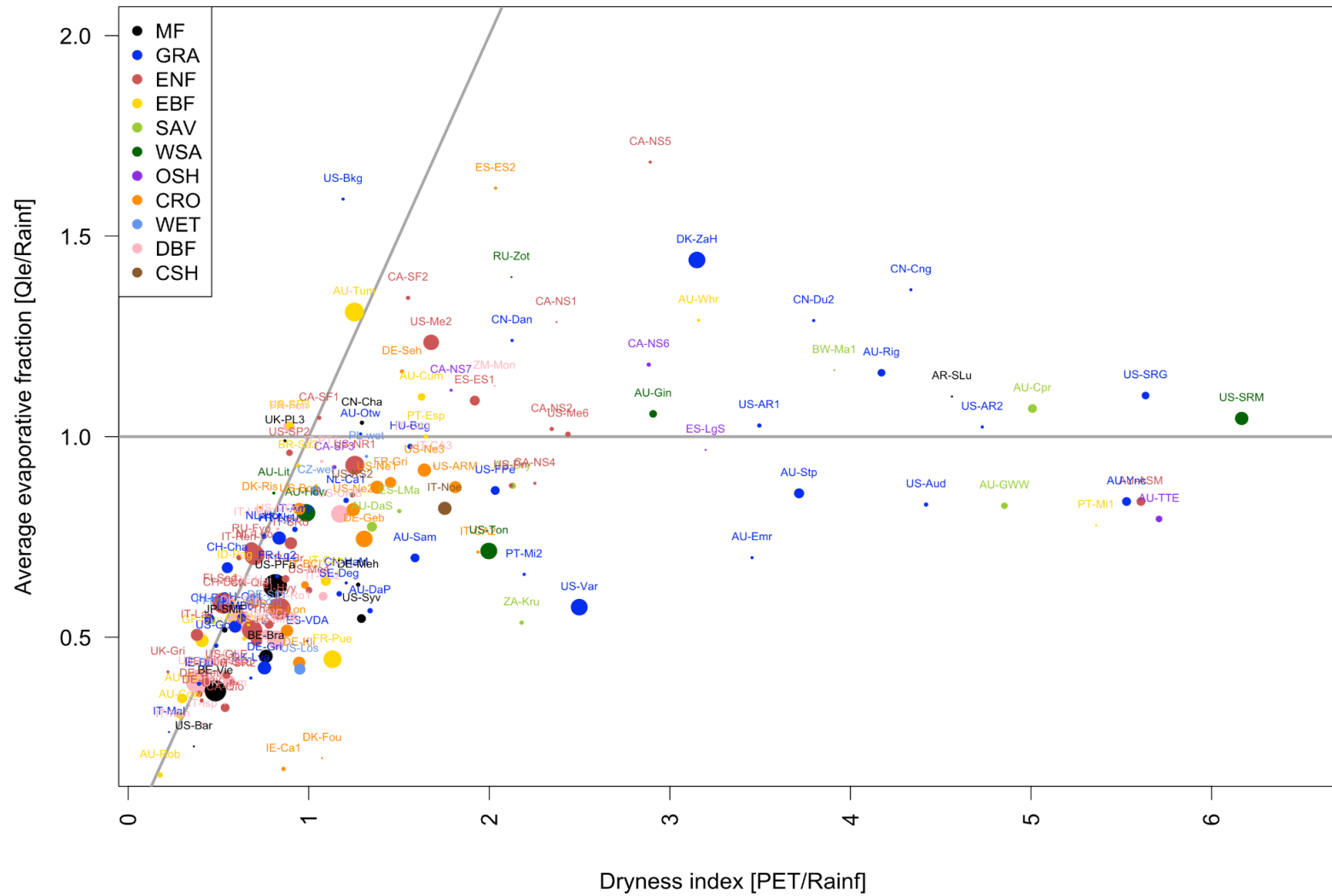
Figure S2a: Distribution of site IGBP vegetation types on a Budyko style plot, using raw (uncorrected) fluxes for all 170 sites. Dot sizes indicate the length of site data, ranging from 1 (shortest) to 21 years (longest) - see Table S2 below for site details. Vegetation types are: Mixed Forest (MF); Grassland (GRA); Evergreen Needleleaf (ENF); Evergreen Broadleaf (EBF); Savanna (SAV); Woody Savanna (WSA); Open Shrubland (OSH); Cropland (CRO); Wetland (WET); Deciduous Broadleaf (DBF); Closed Shrubland (CSH).
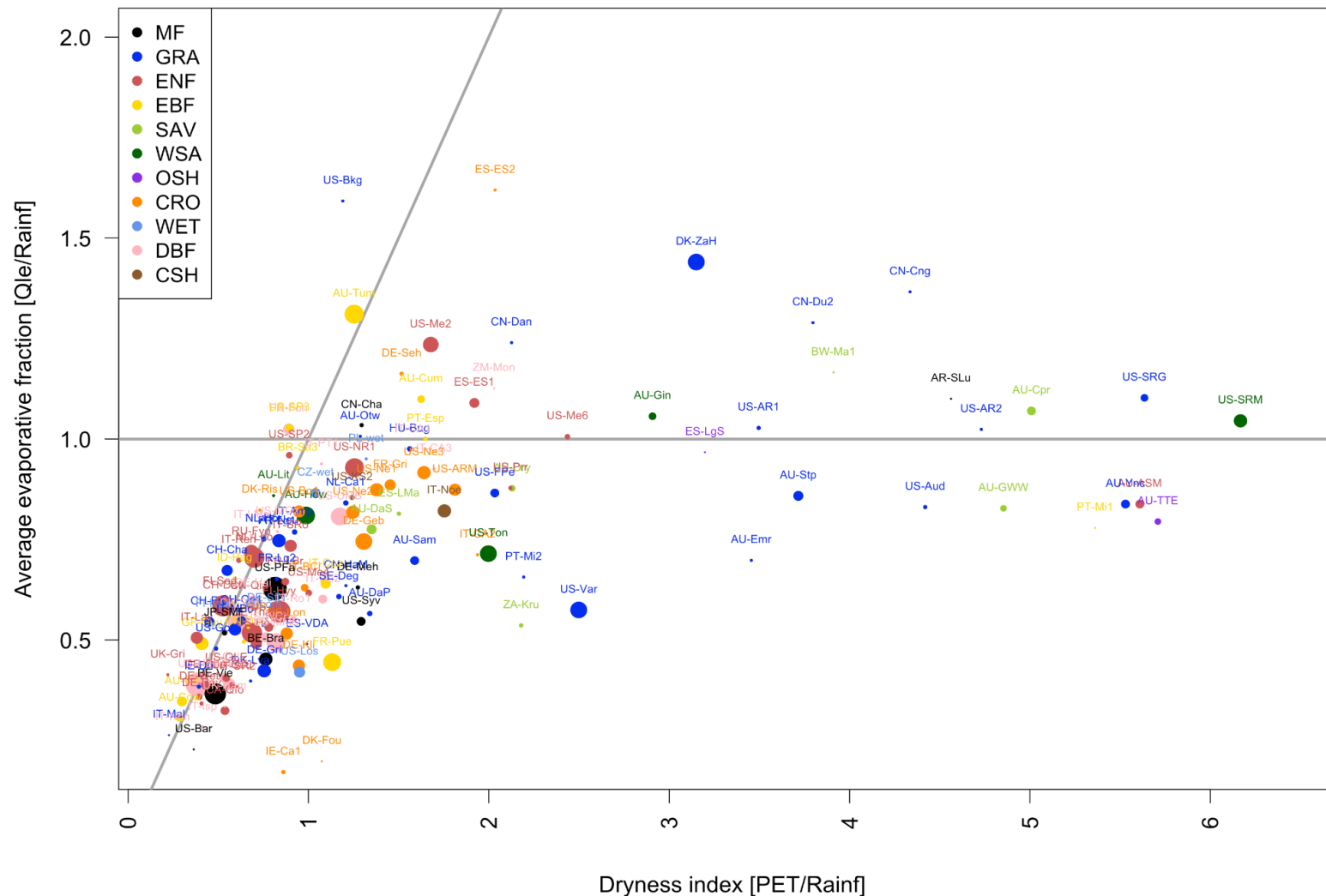
Figure S2b: Distribution of site IGBP vegetation types on a Budyko style plot, using raw (uncorrected) fluxes for 154 sites, that is with 16 of 170 removed because of precipitation issues. Dot sizes indicate the length of site data, ranging from 1 (shortest) to 21 years (longest) - see Table S2 below for site details. Vegetation types are: Mixed Forest (MF); Grassland (GRA); Evergreen Needleleaf (ENF); Evergreen Broadleaf (EBF); Savanna (SAV); Woody Savanna (WSA); Open Shrubland (OSH); Cropland (CRO); Wetland (WET); Deciduous Broadleaf (DBF); Closed Shrubland (CSH).
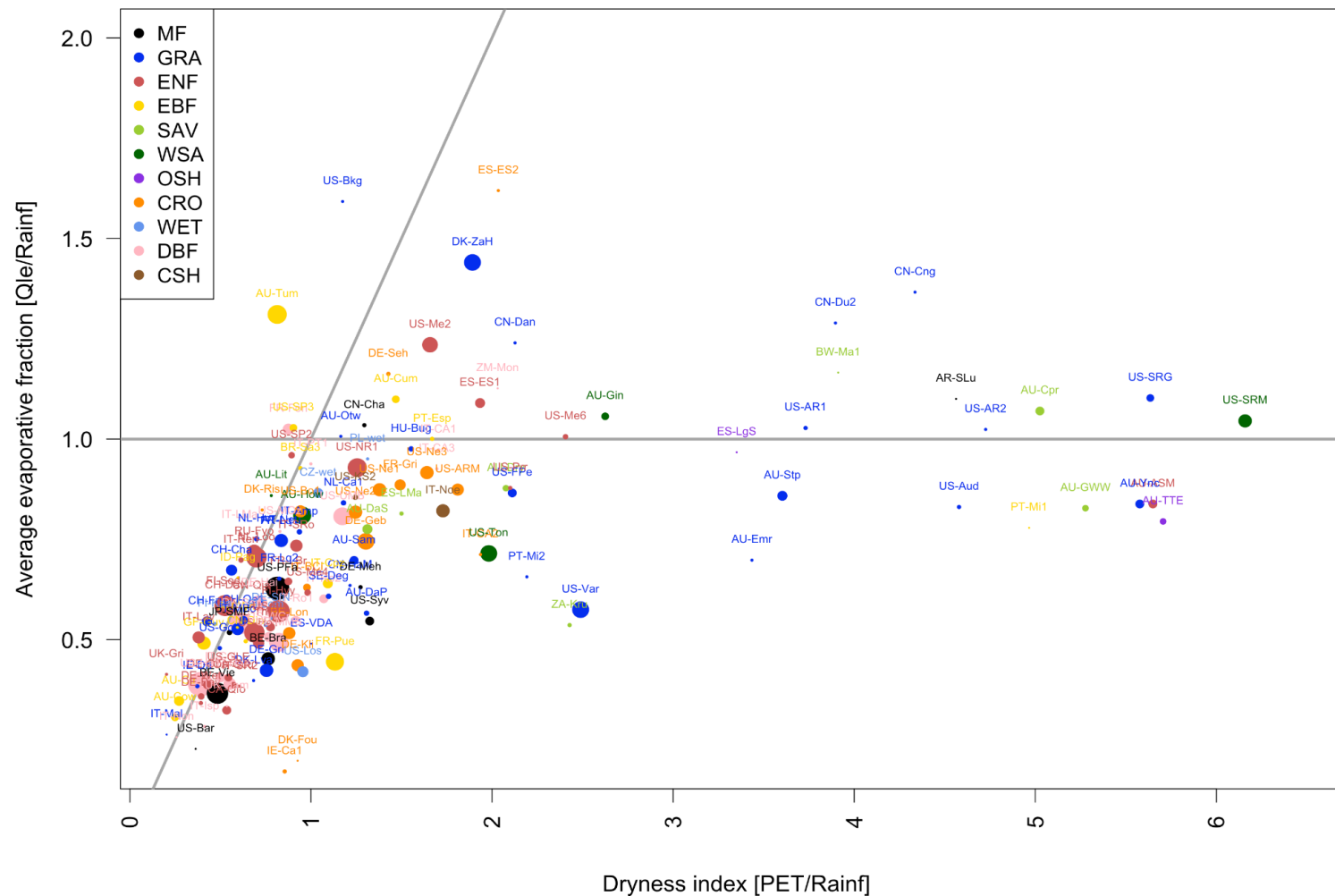
Figure S2c: Distribution of site IGBP vegetation types on a Budyko style plot, using raw (uncorrected) fluxes for 154 sites, similar to Figure S2b, but using all time steps from sites, rather than removing Qle timesteps that had been gap-filled. Results are broadly similar to Figure S2b. Dot sizes indicate the length of site data, ranging from 1 (shortest) to 21 years (longest) - see Table S2 below for site details. Vegetation types are: Mixed Forest (MF); Grassland (GRA); Evergreen Needleleaf (ENF); Evergreen Broadleaf (EBF); Savanna (SAV); Woody Savanna (WSA); Open Shrubland (OSH); Cropland (CRO); Wetland (WET); Deciduous Broadleaf (DBF); Closed Shrubland (CSH)
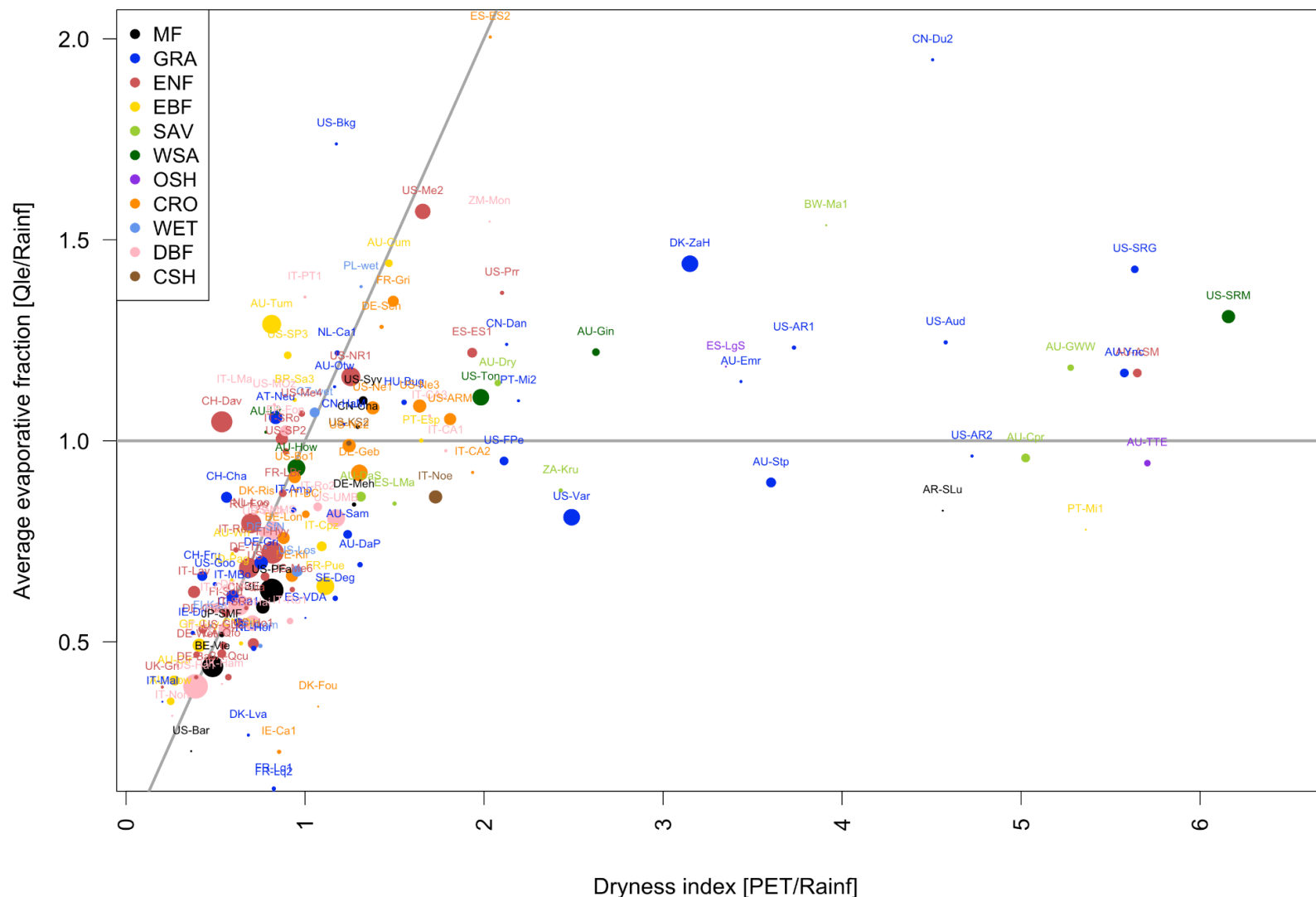
Figure S2d: Distribution of site IGBP vegetation types on a Budyko style plot, using energy balance corrected fluxes using the Fluxnet2015 algorithm, for 154 sites . Dot sizes indicate the length of site data, ranging from 1 (shortest) to 21 years (longest) - see Table S2 below for site details. Vegetation types are: Mixed Forest (MF); Grassland (GRA); Evergreen Needleleaf (ENF); Evergreen Broadleaf (EBF); Savanna (SAV); Woody Savanna (WSA); Open Shrubland (OSH); Cropland (CRO); Wetland (WET); Deciduous Broadleaf (DBF); Closed Shrubland (CSH)
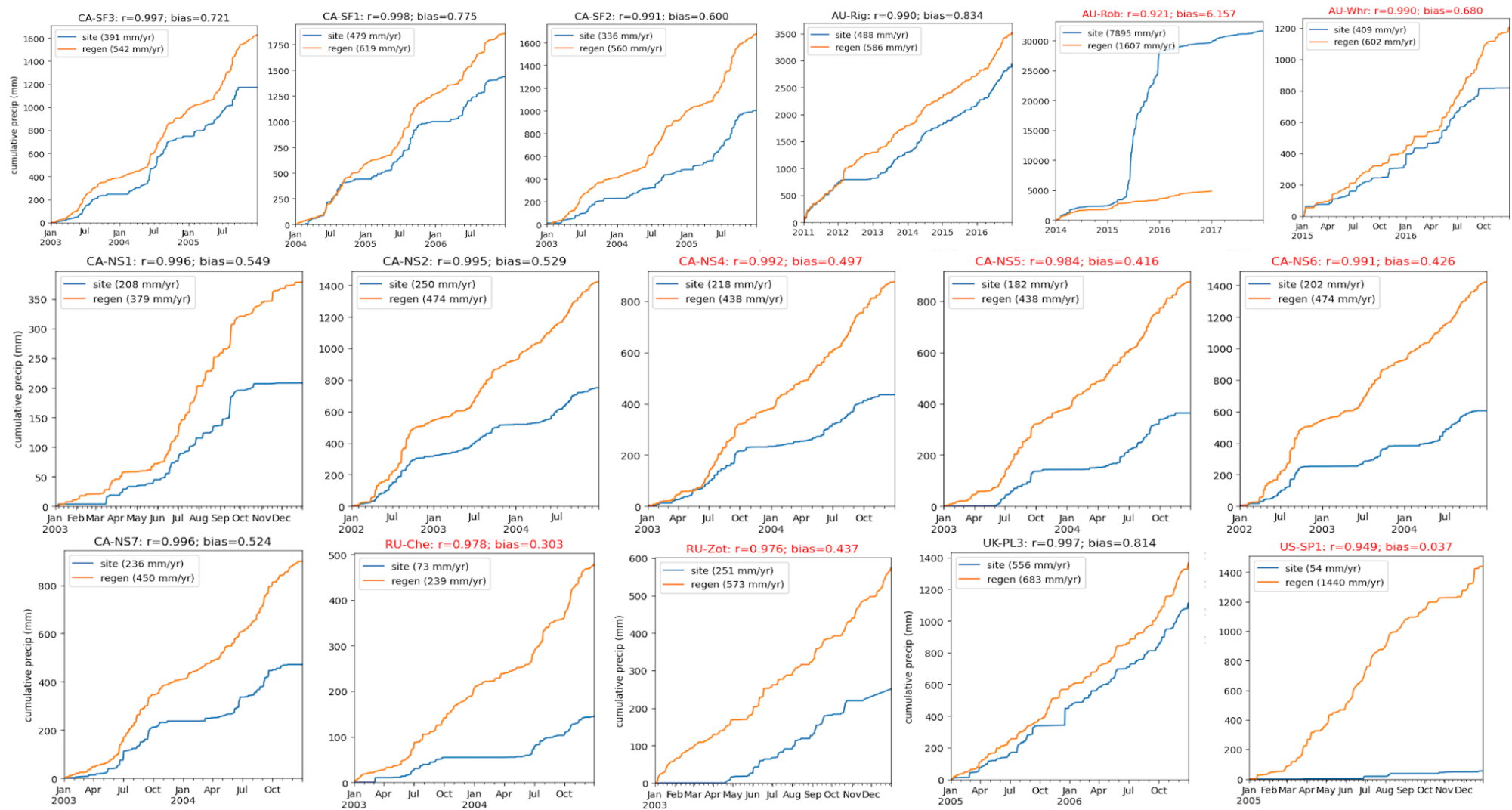
Figure S3: Cumulative site measured precipitation versus REGEN precipitation for the containing grid cell at the 16 sites excluded from this study for precipitation inconsistencies. Red text indicates sites with (arbitrarily chosen) thresholds of correlation < 0.99 or ratio bias b/w REGEN and site data of > 20%.

Table S1: ALMA standard names, their definitions, and relationship to CMIP and CF-netCDF standards. This is a new iteration of the standard originally detailed by Polcher et al, (1998; 2000), and is also available on modelevaluation.org.

short_name _alma	short_name_cmip	CF standard_name	long_name	Definition / notes	unit	direction	dim	grp_ cmip
SWnet	rss	surface_net_downward_shortwave_flux	Net shortwave radiation	Incoming solar radiation less the simulated outgoing shortwave radiation, averaged over a grid cell	W/m2	Down	XYT	LEday
LWnet	rls	surface_net_downward_longwave_flux	Net longwave radiation	Incident longwave radiation less the simulated outgoing longwave radiation, averaged over a grid cell	W/m2	Down	XYT	LEday
SWdown	rsds	surface_downwelling_shortwave_flux_in_air	Downward short-wave radiation		W/m2	Down	XYT	LEday
LWdown	rlds	surface_downwelling_longwave_flux_in_air	Downward long-wave radiation		W/m2	Down	XYT	LEday
SWup	rsus	surface_upwelling_shortwave_flux_in_air	Upward short-wave radiation		W/m2	Up	XYT	LEday
LWup	rlus	surface_upwelling_longwave_flux_in_air	Upward long-wave radiation	This upward longwave flux is to be compared to an ISCCP derived product.	W/m2	Up	XYT	LEday
Qle	hfls	surface_upward_latent_heat_flux	Latent heat flux	Energy of evaporation, averaged over a grid cell	W/m2	Up	XYT	LEday
Qh	hfss	surface_upward_sensible_heat_flux	Sensible heat flux	Sensible energy, averaged over a grid cell	W/m2	Up	XYT	LEday
Qg	hfds	surface_downward_heat_flux	Ground heat flux	Heat flux into the ground, averaged over a grid cell	W/m2	Down	XYT	LEday
Qgs	hfdsn	surface_downward_heat_flux_in_snow	Downward heat flux into snow		W/m2	Down	XYT	LEday
Qf	hfmlt	surface_snow_and_ice_melt_heat_flux	Energy of fusion	Energy consumed or released during liquid/solid phase changes.	W/m2	Soild to Liquid	XYT	LEday
Qv	hfsbl	surface_snow_and_ice_sublimation_heat_flux	Energy of sublimation	Energy consumed or released during vapor/solid phase changes.	W/m2	Soild to Vapor	XYT	LEday
Qtau	tau	surface_downward_stress	Momentum flux	module of the momentum lost by the atmosphere to the surface.	N/m2	Down	XYT	LEday
Qa	hfrs	temperature_flux_due_to_rainfall_expressed_as_heat_flux_onto_snow_and_ice	Heat transferred to snowpack by rainfall	Heat transferred to a snow cover by rain.	W/m2	Down	XYT	LEday
DelSurfHeat	dtes	change_over_time_in_thermal_energy_content_of_surface	Change in surface heat storage	Change in heat storage over the soil layer and the vegetation for which the energy balance is calculated, accumulated over the sampling time interval.	J/m2	Increase	XYT	LEday

DelColdCont	dtesn	change_over_time_in_thermal_energy_content_of_surface_snow_and_ice	Change in snow/ice cold content	Change in cold content over the snow layer for which the energy balance is calculated, accumulated over the sampling time interval. This should also include the energy contained in the liquid water in the snow pack.	J/m2	Increase	XYT	LEday
AvgSurfT	ts	surface_temperature	Average surface temperature	Average of all vegetation, bare soil and snow skin temperatures	K	-	XYT	LEday
SnowT	tsns	surface_snow_skin_temperature	Snow Surface Temperature	Temperature of the snow surface as it interacts with the atmosphere, averaged over a grid cell.	K	-	XYT	LEday
VegT	tcs	surface_canopy_skin_temperature	Vegetation Canopy Temperature	Vegetation temperature, averaged over all vegetation types	K	-	XYT	LEday
BaresoilT	tgs	surface_ground_skin_temperature	Temperature of bare soil	Surface bare soil temperature	K	-	XYT	LEday
RadT	tr	surface_radiative_temperature	Surface Radiative Temperature	Effective radiative surface temperature, averaged over the grid cell	K	-	XYT	LEday
Albedo	albs	surface_albedo	Surface Albedo	Grid cell average albedo for all wavelengths.	-	-	XYT	LEday
SAlbedo	albsn	snow_and_ice_albedo	Snow Albedo	Albedo of the snow-covered surface, averaged over the grid cell.	-	-	XYT	LEday
SnowFrac	snc	surface_snow_area_fraction	Snow covered fraction	Grid cell snow covered fraction	-	-	XYT	LEday
CAlbedo	albc	canopy_albedo	Canopy Albedo		-	-	XYT	LEday
CanoFrac	cnc	surface_canopy_area_fraction	Canopy covered fraction		-	-	XYT	LEday
SoilTemp	tsl	soil_temperature	Average layer soil temperature	Average soil temperature in each user-defined soil layer (3D variable)	K	-	XYZT	LEday
SnowTProf	tsnl	snow_temperature	Temperature profile in the snow	Temperature in the snow pack present in the grid-cell. 3D variable for multi-layer snow schemes.	K	-	XYZT	LEday
TairMax	tasmax	air_temperature_maximum	Daily Maximum Near-Surface Air Temperature		K	-	XYT	LEday
TairMin	tasmin	air_temperature_minimum	Daily Minimum Near-Surface Air Temperature		K	-	XYT	LEday
CCover	clt	cloud_area_fraction	Total cloud fraction		-	-	XYT	LEday
Precip	pr	precipitation_flux	Precipitation rate		kg/m2/s	Down	XYT	LWday
Rainf	prra	rainfall_flux	Rainfall rate		kg/m2/s	Down	XYT	LWday
Snowf	prsn	snowfall_flux	Snowfall rate		kg/m2/s	Down	XYT	LWday
CRainf	prrc	convective_rainfall_flux	Convective Rainfall rate		kg/m2/s	Down	XYT	LWday
CSnowf	prsnc	convective_snowfall_flux	Convective Snowfall rate		kg/m2/s	Down	XYT	LWday
PrecipCanop	prveg	precipitation_flux_onto_canopy	Precipitation onto canopy		kg/m2/s	Down	XYT	LWday
Evap	et	surface_evapotranspiration	Total Evapotranspiration		kg/m2/s	Up	XYT	LWday
ECanop	ec	liquid_water_evaporation_flux_from_canopy	Interception evaporation		kg/m2/s	Up	XYT	LWday
TVeg	tran	Transpiration	Vegetation transpiration		kg/m2/s	Up	XYT	LWday
ESoil	es	liquid_water_evaporation_flux_from_soil	Bare soil evaporation		kg/m2/s	Up	XYT	LWday

EWater	eow	liquid_water_evaporation_flux_from_open_water	Open water evaporation		kg/m2/s	Up	XYT	LWday
EvapSnow	esn	liquid_water_evaporation_flux_from_surface_snow	Snow Evaporation		kg/m2/s	Up	XYT	LWday
SubSnow	sbl	surface_snow_and_ice_sublimation_flux	Snow sublimation		kg/m2/s	Up	XYT	LWday
SubSurf	slbnosn	sublimation_amount_assuming_no_snow	Sublimation of the snow free area		kg/m2/s	Up	XYT	LWday
PotEvap	potet	water_potential_evapotranspiration_flux	Potential Evapotranspiration		kg/m2/s	Up	XYT	LWday
Qr	mrro	runoff_flux	Total runoff		kg/m2/s	Out	XYT	LWday
Qs	mrros	surface_runoff_flux	Surface runoff		kg/m2/s	Out	XYT	LWday
Qsb	mrrob	subsurface_runoff_flux	Subsurface runoff		kg/m2/s	Out	XYT	LWday
Qsm	snm	surface_snow_and_ice_melt_flux	Snowmelt		kg/m2/s	Solid to liquid	XYT	LWday
Qfz	snrefr	surface_snow_and_ice_refreezing_flux	Re-freezing of water in the snow		kg/m2/s	Liquid to solid	XYT	LWday
Qst	snmsl	surface_snow_melt_flux_into_soil_layer	Water flowing out of snowpack		kg/m2/s	Out	XYT	LWday
Qgwr	qgwr	water_flux_from_soil_layer_to_groundwater	Groundwater recharge from soil layer		kg/m2/s	Out	XYT	LWday
Qrec			Recharge from river to flood plain		kg/m2/s	Out	XYT	LWday
Inf	rivi	water_flux_from_upstream	River Inflow		m3/s	In	XYT	LWday
Dis	rivo	water_flux_to_downstream	River Discharge		m3/s	Out	XYT	LWday
DelSoilMoist	dslw	change_over_time_in_mass_content_of_water_in_soil	Change in soil moisture	Change in the simulated vertically integrated soil water volume, averaged over a grid cell, accumulated over the sampling time interval.	kg/m2	Increase	XYT	LWday
DelSWE	dsn	change_over_time_in_surface_snow_and_ice_amount	Change in snow water equivalent		kg/m2	Increase	XYT	LWday
DelSurfStor	dsw	change_over_time_in_surface_water_amount	Change in Surface Water Storage		kg/m2	Increase	XYT	LWday
DelIntercept	dcw	change_over_time_in_canopy_water_amount	Change in interception storage		kg/m2	Increase	XYT	LWday
DelGW	dgw	change_over_time_in_groundwater	Change in groundwater		kg/m2	Increase	XYT	LWday
DelRivStor	drivw	change_over_time_in_river_water_amount	Change in river storage		kg/m2	Increase	XYT	LWday
RootMoist	rzwc	water_content_of_root_zone	Root zone soil moisture		kg/m2	-	XYT	LWday
CanopInt	cw	canopy_water_amount	Total canopy water storage		kg/m2	-	XYT	LWday

SWE	snw	surface_snow_amount	Snow Water Equivalent	Total water mass of the snowpack (liquid or frozen), averaged over a grid cell. 3D variable for multi-layer snow schemes.	kg/m2	-	XYZT	LWday
SWEVeg	snwc	canopy_snow_amount	SWE intercepted by the vegetation	Total water mass of the snowpack (liquid or frozen), averaged over a grid cell and intercepted by the canopy.	kg/m2	-	XYT	LWday
LiqSnow	lwsnl	liquid_water_content_of_snow_layer	Liquid water in snow pack		kg/m2	-	XYZT	LWday
SurfStor	sw	surface_water_amount_assuming_no_snow	Surface Water Storage	Total liquid water storage, other than soil, snow or interception storage (i.e. lakes, river channel or depression storage).	kg/m2	-	XYT	LWday
	mrso	mass_content_of_water_in_soil	Soil Moisture					
SoilMoist	mrlsl	moisture_content_of_soil_layer	Average layer soil moisture	Soil water content in each user-defined soil layer (3D variable). Includes the liquid, vapor and solid phases of water in the soil.	kg/m2	-	XYZT	LWday
SoilMoistTop	mrsos	moisture_content_of_soil_layer	Moisture in top soil (10cm) layer		kg/m2	-	XYT	LWday
SoilWet	mrsow	relative_soil_moisture_content_above_wilting_point	Total Soil Wetness	Vertically integrated soil moisture divided by maximum allowable soil moisture above wilting point.	-	-	XYT	LWday
WaterTableD	wtd	depth_of_soil_moisture_saturation	Water table depth		m	-	XYT	LWday
TWS	tws	canopy_and_surface_and_subsurface_water_amount	Terrestrial Water Storage		kg/m2	-	XYT	LWday
SMLiqFrac	mrlqso	mass_fraction_of_unfrozen_water_in_soil_layer	Average layer fraction of liquid moisture	Fraction of soil moisture mass in the liquid phase in each user-defined soil layer (3D variable)	-	-	XYZT	LWday
SMFrozFrac	mrfsofr	mass_fraction_of_frozen_water_in_soil_layer	Average layer fraction of frozen moisture	Fraction of soil moisture mass in the solid phase in each user-defined soil layer (3D variable)	-	-	XYZT	LWday
RainfSnowFrac	prrsn	mass_fraction_of_rainfall_onto_snow	Fraction of rainfall on snow.	The fraction of the grid averaged rainfall which falls on the snow pack	-	-	XYT	LWday
SnowfSnowFrac	prsnsn	mass_fraction_of_snowfall_onto_snow	Fraction of snowfall on snow.	The fraction of the snowfall which falls on the snow pack	-	-	XYT	LWday
SliqFrac	lqsn	mass_fraction_of_liquid_water_in_snow	Snow liquid fraction	Fraction of Snow Equivalent Water which is in the liquid phase. 3D variable for multi-layer snow schemes.	-	-	XYZT	LWday
SnowDepth	snd	surface_snow_thickness	Depth of snow layer	Depth of each layer of snow is a 3D variable for multi-layer snow schemes and the total snow depth for simpler models.	m	-	XYT	LWday
SnowAge	agesno	age_of_surface_snow	Snow Age		day	-	XYT	LWday
SnowSoot	sootsn	soot_content_of_surface_snow	Snow Soot Content		kg/m2	-	XYT	LWday
IceFrac	sic	sea_ice_area_fraction	Ice-covered fraction	The fraction of the grid cell covered by sea-ice	-	-	XYT	LWday
IceT	sit	sea_ice_thickness	Sea-ice thickness	The thickness of the ice layer on simulated water areas.	m	-	XYT	LWday

Fdepth	dfr	depth_of_frozen_soil	Frozen soil depth	Depth from surface to the first zero degree isotherm. Above this isotherm T < 0o, and below this line T > 0o.	m	Down	XYT	LWday
Tdepth	dmlt	depth_of_subsurface_melting	Depth to soil thaw	Depth from surface to the zero degree isotherm. Above this isotherm T > 0o, and below this line T < 0o.	m	Down	XYT	LWday
PermafrostT	tpf	permafrost_layer_thickness	Permafrost Layer Thickness		m	-	XYT	LWday
LiqPermafrost	pflw	liquid_water_content_of_permafrost_layer	Liquid water content of permafrost layer		kg/m2	-	XYT	LWday
ACond			Aerodynamic conductance		m/s	-	XYT	LWday
AResist	ares	aerodynamic_resistance	Aerodynamic resistance		s/m	-	XYT	LWday
NudgIncSoilMoist	nudginc_sm	nudging_increment_in_water_content_of_soil_layer	Nudging Increment of Water in Soil Moisture		kg/m2	Increase	XYT	
NudgIncSWE	nudginc_swe	nudging_increment_in_surface_snow_and_ice_amount	Nudging Increment of Water in Snow	Total water storage change due to nudging in LFMIP	kg/m2	Increase	XYT	
RH	hur	relative_humidity	Relative humidity		%	-	XYT	LWday
RHMax	hurmax	relative_humidity_maximum	Daily Maximum Near-Surface Relative Humidity		%	-	XYT	LWday
RHMin	hurmin	relative_humidity_minimum	Daily Minimum Near-Surface Relative Humidity		%	-	XYT	LWday
GPP	gpp	gross_primary_productivity_of_carbon	Gross Primary Production	Carbon Mass Flux out of Atmosphere due to Gross Primary Production on Land	kg/m2/s	Down	XYT	LCmon
NPP	npp	net_primary_productivity_of_carbon	Net Primary Production	Carbon Mass Flux out of Atmosphere due to Net Primary Production on Land	kg/m2/s	Down	XYT	LCmon
NEE	nep	surface_net_downward_mass_flux_of_carbon_dioxide_expressed_as_carbon_due_to_all_land_processes_excluding_anthropogenic_land_use_change	Net Ecosystem Exchange	Net Carbon Mass Flux out of Atmosphere due to Net Ecosystem Productivity on Land.	kg/m2/s	Down	XYT	LCmon
AutoResp	ra	plant_respiration_carbon_flux	Autotrophic Respiration	Carbon Mass Flux into Atmosphere due to Autotrophic (Plant) Respiration on Land; Autotrophic respiration includes maintenance respiration and growth respiration	kg/m2/s	Up	XYT	LCmon
HeteroResp	rh	heterotrophic_respiration_carbon_flux	Heterotrophic Respiration	Carbon Mass Flux into Atmosphere due to Heterotrophic Respiration on Land	kg/m2/s	Up	XYT	LCmon
	fLuc	surface_net_upward_mass_flux_of_carbon_dioxide_expressed_as_carbon_due_to_emission_from_anthropogenic_land_use_change	Net Carbon Mass Flux into Atmosphere due to Land Use Change	human changes to land (excluding forest regrowth) accounting possibly for different time-scales related to fate of the wood, for example.	kg/m2/s	Up	XYT	LCmon
TotLivBiom			Total Living Biomass	Total carbon content of the living biomass	kg/m2	-	XYT	LCmon
TotSoilCarb	cSoil	soil_carbon_content	Carbon Mass in Soil Pool	Total soil and litter carbon content integrated over the entire soil profile	kg/m2	-	XYT	LCmon

	cLitter	litter_carbon_content	Carbon Mass in Litter Pool		kg/m2	-	XYT	LCmon
	cVeg	vegetation_carbon_content	Carbon Mass in Vegetation		kg/m2	-	XYT	LCmon
	cProduct	carbon_content_of_products_of_anthropogenic_land_use_change	Carbon Mass in Products of Land Use Change		kg/m2	-	XYT	LCmon
	cLeaf	leaf_carbon_content	Carbon Mass in Leaves		kg/m2	-	XYT	LCmon
	cWood	wood_carbon_content	Carbon Mass in Wood		kg/m2	-	XYT	LCmon
	cRoot	root_carbon_content	Carbon Mass in Roots		kg/m2	-	XYT	LCmon
	cMisc	miscellaneous_living_matter_carbon_content	Carbon Mass in Other Living Compartments on Land		kg/m2	-	XYT	LCmon
	fVegLitter	litter_carbon_flux	Total Carbon Mass Flux from Vegetation to Litter		kg/m2/s	-	XYT	LCmon
	fLitterSoil	carbon_mass_flux_into_soil_from_litter	Total Carbon Mass Flux from Litter to Soil		kg/m2/s	-	XYT	LCmon
	fVegSoil	carbon_mass_flux_into_soil_from_vegetation_excluding_litter	Total Carbon Mass Flux from Vegetation Directly to Soil		kg/m2/s	-	XYT	LCmon
	treeFrac	area_fraction	Tree Cover Fraction	fraction of entire grid cell that is covered by trees.	%	-	XYT	LCmon
	grassFrac	area_fraction	Natural Grass Fraction	fraction of entire grid cell that is covered by natural grass.	%	-	XYT	LCmon
	shrubFrac	area_fraction	Shrub Fraction	fraction of entire grid cell that is covered by shrub.	%	-	XYT	LCmon
	cropFrac	area_fraction	Crop Fraction	fraction of entire grid cell that is covered by crop.	%	-	XYT	LCmon
	pastureFrac	area_fraction	Anthropogenic Pasture Fraction	fraction of entire grid cell that is covered by anthropogenic pasture.	%	-	XYT	LCmon
	baresoilFrac	area_fraction	Bare Soil Fraction	fraction of entire grid cell that is covered by bare soil.	%	-	XYT	LCmon
	residualFrac	area_fraction	Fraction of Grid Cell that is Land but Neither Vegetation-Covered nor Bare Soil	fraction of entire grid cell that is land and is covered by "non-vegetation" and "non-bare-soil" (e.g., urban, ice, lakes, etc.)	%	-	XYT	LCmon
LAI	lai	leaf_area_index	Leaf Area Index	a ratio obtained by dividing the total upper leaf surface area of vegetation by the (horizontal) surface area of the land on which it grows.	-	-	XYT	LCmon
SWdown	rsds	surface_downwelling_shortwave_flux_in_air	Downward short-wave radiation		W/m2	Down	XYT	L3hr
LWdown	rlds	surface_downwelling_longwave_flux_in_air	Downward long-wave radiation		W/m2	Down	XYT	L3hr

Qair	huss	specific_humidity	Near surface specific humidity		kg/kg	-		XYT	L3hr
Tair	ta	air_temperature	Near surface air temperature		K	-		XYT	L3hr
Psurf	ps	surface_air_pressure	Surface Pressure		Pa	-		XYT	L3hr
Wind	ws	wind_speed	Near surface wind speed		m/s	-		XYT	L3hr
Wind_N	va	northward_wind	Near surface northward wind component		m/s	North		XYT	L3hr
Wind_E	ua	eastward_wind	Near surface eastward wind component		m/s	East		XYT	L3hr
Precip	pr	precipitation_flux	Precipitation rate		kg/m2/s	Down		XYT	L3hr
Rainf	prr	rainfall_flux	Rainfall rate		kg/m2/s	Down		XYT	L3hr
Snowf	prsn	snowfall_flux	Snowfall rate		kg/m2/s	Down		XYT	L3hr
CRainf	prrc	convective_rainfall_flux	Convective Rainfall rate		kg/m2/s	Down		XYT	L3hr
CSnowf	prsnc	convective_snowfall_flux	Convective Snowfall rate		kg/m2/s	Down		XYT	L3hr
CCover	clt	cloud_area_fraction	Total cloud fraction		-	-		XYT	L3hr
CO2air	co2c	mole_fraction_of_carbon_dioxide_in_air	Near surface CO2 concentration		-	-		XYT	L3hr

Table S2: List of 170 sites used for PLUMBER2 (from Ukkola et al, 2022), site properties and references. Each site has a more detailed profile with additional references on modelevaluation.org. More information from www.ozflux.org.au and fluxnet.org. Vegetation types are: Mixed Forest (MF); Grassland (GRA); Evergreen Needleleaf (ENF); Evergreen Broadleaf (EBF); Savanna (SAV); Woody Savanna (WSA); Open Shrubland (OSH); Cropland (CRO); Wetland (WET); Deciduous Broadleaf (DBF); Closed Shrubland (CSH)

Fluxnet site code	Time period	IGBP veg type	Veg height (m)	Ref height (m)	Elevation (m)	Data source	Default LAI
AR-SLu	2010	MF	4.5	11	500	FLUXNET2015	MODIS
AT-Neu	2002-2012	GRA	1	3	970	FLUXNET2015	Copernicus
AU-ASM	2011-2017	ENF	6.5	11.6	606	OzFlux	Copernicus
AU-Cow	2010-2015	EBF	22	35	86	OzFlux	Copernicus
AU-Cpr	2011-2017	SAV	4	20	76	OzFlux	MODIS
AU-Ctr	2010-2017	EBF	25	45	66	OzFlux	MODIS
AU-Cum	2013-2018	EBF	23	30	200	OzFlux	MODIS
AU-DaP	2011-2017	GRA	0.3	15	116	OzFlux	Copernicus
AU-DaS	2010-2017	SAV	16.4	21	108	OzFlux	MODIS
AU-Dry	2011-2015	SAV	12.3	15	191	OzFlux	Copernicus
AU-Emr	2012-2013	GRA	2	5.6	177	OzFlux	Copernicus
AU-Gin	2012-2017	WSA	7	15	51	OzFlux	MODIS
AU-GWW	2013-2017	SAV	18	35	504	OzFlux	MODIS
AU-How	2003-2017	WSA	16	23	41	OzFlux	MODIS
AU-Lit	2016-2017	WSA	20	31	200	OzFlux	Copernicus
AU-Otw	2009-2010	GRA	0.1	10	54	OzFlux	Copernicus
AU-Rig	2011-2016	GRA	0.4	2.5	133	OzFlux	MODIS
AU-Rob	2014-2017	EBF	35	40	710	OzFlux	Copernicus
AU-Sam	2011-2017	GRA	0.5	2	170	OzFlux	Copernicus
AU-Stp	2010-2017	GRA	0.5	4.8	252	OzFlux	Copernicus
AU-TTE	2013-2017	OSH	4.85	9.81	553	OzFlux	MODIS
AU-Tum	2002-2017	EBF	40	70	1200	OzFlux	Copernicus
AU-Whr	2015-2016	EBF	28	32	152	OzFlux	MODIS
AU-Wrr	2016-2017	EBF	55	80	100	OzFlux	MODIS
AU-Ync	2011-2017	GRA	0.5	8	125	OzFlux	Copernicus
BE-Bra	2004-2014	MF	21	39	16	FLUXNET2015	MODIS
BE-Lon	2005-2014	CRO	1	2.7	167	FLUXNET2015	Copernicus

BE-Vie	1997-2014	MF	35	40	493	FLUXNET2015	Copernicus
BR-Sa3	2001-2003	EBF	40	64	100	FLUXNET2015	MODIS
BW-Ma1	2000	SAV	8	12.6	929	LaThuile	MODIS
CA-NS1	2003	ENF	20	24	260	FLUXNET2015	MODIS
CA-NS2	2002-2004	ENF	20	20	260	FLUXNET2015	Copernicus
CA-NS4	2003-2004	ENF	7	10	260	FLUXNET2015	MODIS
CA-NS5	2003-2004	ENF	5	9	260	FLUXNET2015	MODIS
CA-NS6	2002-2004	OSH	4	6	244	FLUXNET2015	MODIS
CA-NS7	2003-2004	OSH	0.25	6	297	FLUXNET2015	MODIS
CA-Qcu	2002-2006	ENF	5.5	7	392	LaThuile	Copernicus
CA-Qfo	2004-2010	ENF	14	24	382	FLUXNET2015	Copernicus
CA-SF1	2004-2006	ENF	6	12	536	FLUXNET2015	MODIS
CA-SF2	2003-2005	ENF	4	10	520	FLUXNET2015	MODIS
CA-SF3	2003-2005	OSH	1	20	540	FLUXNET2015	Copernicus
CH-Cha	2006-2014	GRA	0.5	2	393	FLUXNET2015	Copernicus
CH-Dav	1997-2014	ENF	25	35	1639	FLUXNET2015	Copernicus
CH-Fru	2007-2014	GRA	0.5	2.55	982	FLUXNET2015	MODIS
CH-Oe1	2002-2008	GRA	0.5	2	450	FLUXNET2015	MODIS
CN-Cha	2003-2005	MF	28	40	754	FLUXNET2015	MODIS
CN-Cng	2008-2009	GRA	0.75	2	138	FLUXNET2015	MODIS
CN-Dan	2004-2005	GRA	1	2.1	4751	FLUXNET2015	MODIS
CN-Din	2003-2005	EBF	30	27	261	FLUXNET2015	Copernicus
CN-Du2	2007-2008	GRA	0.5	3	1331	FLUXNET2015	MODIS
CN-HaM	2002-2003	GRA	0.3	2.2	3975	FLUXNET2015	MODIS
CN-Qia	2003-2005	ENF	13	39.6	64	FLUXNET2015	MODIS
CZ-wet	2007-2014	WET	1	2.7	426	FLUXNET2015	MODIS
DE-Bay	1997-1999	ENF	25	31	781	LaThuile	Copernicus
DE-Geb	2001-2014	CRO	1	6	161.5	FLUXNET2015	Copernicus
DE-Gri	2004-2014	GRA	0.7	3	385	FLUXNET2015	Copernicus
DE-Hai	2000-2012	DBF	33	43.5	430	FLUXNET2015	Copernicus
DE-Kli	2005-2014	CRO	1.5	3.5	478	FLUXNET2015	Copernicus
DE-Meh	2004-2006	MF	1	3	291	LaThuile	MODIS

DE-Obe	2008-2014	ENF	19	30	734	FLUXNET2015	Copernicus
DE-Seh	2008-2010	CRO	0.8	2	103	FLUXNET2015	Copernicus
DE-SfN	2013-2014	WET	2	4.3	590	FLUXNET2015	Copernicus
DE-Tha	1998-2014	ENF	26.5	42	380	FLUXNET2015	Copernicus
DE-Wet	2002-2006	ENF	22	29.4	703	LaThuile	MODIS
DK-Fou	2005	CRO	1	3.5	51	FLUXNET2015	MODIS
DK-Lva	2005-2006	GRA	0.5	2.5	-2493	LaThuile	Copernicus
DK-Ris	2004-2005	CRO	1	2	24	LaThuile	MODIS
DK-Sor	1997-2014	DBF	25	57	40	FLUXNET2015	Copernicus
DK-ZaH	2000-2013	GRA	0.5	3	38	FLUXNET2015	MODIS
ES-ES1	1999-2006	ENF	7.5	13	1	LaThuile	MODIS
ES-ES2	2005-2006	CRO	0.5	1.6	7	LaThuile	MODIS
ES-LgS	2007	OSH	0.2	1.5	2267	FLUXNET2015	MODIS
ES-LMa	2004-2006	SAV	8	15	278	LaThuile	MODIS
ES-VDA	2004	SAV	0.5	1.5	1787	LaThuile	MODIS
FI-Hyy	1996-2014	ENF	14	23	181	FLUXNET2015	Copernicus
FI-Kaa	2000-2002	WET	0.8	5	159	LaThuile	MODIS
FI-Lom	2007-2009	WET	0.4	3	274	FLUXNET2015	MODIS
FI-Sod	2008-2014	ENF	12.7	23	180	FLUXNET2015	Copernicus
FR-Fon	2005-2013	DBF	24	35	103	FLUXNET2015	MODIS
FR-Gri	2005-2013	CRO	1	3.17	125	FLUXNET2015	Copernicus
FR-Hes	1997-2006	DBF	13	18	293	LaThuile	Copernicus
FR-LBr	2003-2008	ENF	20	38	61	FLUXNET2015	MODIS
FR-Lq1	2004-2006	GRA	0.5	2	1066	LaThuile	MODIS
FR-Lq2	2004-2006	GRA	0.5	2	1081	LaThuile	MODIS
FR-Pue	2000-2014	EBF	6.5	11	270	FLUXNET2015	MODIS
GF-Guy	2004-2014	EBF	35	55	48	FLUXNET2015	Copernicus
HU-Bug	2003-2006	GRA	1	4	106	LaThuile	MODIS
ID-Pag	2002-2003	EBF	26	41	52	LaThuile	Copernicus
IE-Ca1	2004-2006	CRO	0.9	1.9	72	LaThuile	Copernicus
IE-Dri	2003-2005	GRA	0.5	6	186	LaThuile	Copernicus
IT-Amp	2003-2006	GRA	0.5	4	991	LaThuile	MODIS

IT-BCi	2005-2010	CRO	1	2	20	FLUXNET2015	Copernicus
IT-CA1	2012-2013	DBF	5.5	8	200	FLUXNET2015	MODIS
IT-CA2	2012-2013	CRO	0.3	3.2	200	FLUXNET2015	MODIS
IT-CA3	2012-2013	DBF	3.5	7	197	FLUXNET2015	MODIS
IT-Col	2007-2014	DBF	13	25.2	1560	FLUXNET2015	MODIS
IT-Cpz	2001-2008	EBF	13	15	68	FLUXNET2015	MODIS
IT-Isp	2013-2014	DBF	19	38	210	FLUXNET2015	MODIS
IT-Lav	2005-2014	ENF	28	33	1353	FLUXNET2015	MODIS
IT-LMa	2003-2004	DBF	25	28	350	LaThuile	MODIS
IT-Mal	2003	GRA	0.5	3	1610	LaThuile	MODIS
IT-MBo	2003-2012	GRA	0.3	2.5	1550	FLUXNET2015	MODIS
IT-Noe	2004-2014	CSH	1.2	3	25	FLUXNET2015	MODIS
IT-Non	2002	DBF	7	13	14	LaThuile	MODIS
IT-PT1	2003-2004	DBF	26	30	60	FLUXNET2015	Copernicus
IT-Ren	2010-2013	ENF	28	40	1730	FLUXNET2015	MODIS
IT-Ro1	2002-2006	DBF	15	20	235	FLUXNET2015	MODIS
IT-Ro2	2002-2008	DBF	15	20	160	FLUXNET2015	MODIS
IT-SR2	2013-2014	ENF	19	23.5	4	FLUXNET2015	MODIS
IT-SRo	2003-2012	ENF	16	23.5	6	FLUXNET2015	MODIS
JP-SMF	2003-2006	MF	8.1	19	199	FLUXNET2015	MODIS
NL-Ca1	2003-2006	GRA	0.5	3	1	LaThuile	MODIS
NL-Hor	2008-2011	GRA	1	4.7	2.2	FLUXNET2015	MODIS
NL-Loo	1997-2013	ENF	15.5	27	25	FLUXNET2015	Copernicus
PL-wet	2004-2005	WET	1	2.5	55	LaThuile	MODIS
PT-Esp	2002-2004	EBF	20	33	90	LaThuile	MODIS
PT-Mi1	2005	EBF	7.3	29	230	LaThuile	MODIS
PT-Mi2	2005-2006	GRA	0.1	2.5	193	LaThuile	MODIS
RU-Che	2003-2004	WET	0.4	5.3	6	FLUXNET2015	MODIS
RU-Fyo	2003-2014	ENF	21	48	265	FLUXNET2015	MODIS
RU-Zot	2003	WSA	12	30	124	LaThuile	Copernicus
SD-Dem	2005-2009	SAV	1.5	2.5	500	FLUXNET2015	MODIS
SE-Deg	2002-2005	WET	0.5	1.8	242	LaThuile	Copernicus

UK-Gri	2000-2001	ENF	10	15.4	343	LaThuile	MODIS
UK-Ham	2004	DBF	22	28	76	LaThuile	MODIS
UK-PL3	2005-2006	MF	22	30.5	104	LaThuile	MODIS
US-AR1	2010-2012	GRA	1	2.84	611	FLUXNET2015	Copernicus
US-AR2	2010-2011	GRA	1	2.95	646	FLUXNET2015	Copernicus
US-ARM	2003-2012	CRO	0.5	60	314	FLUXNET2015	Copernicus
US-Aud	2003-2005	GRA	0.5	4	1466	LaThuile	MODIS
US-Bar	2005	MF	21	26.5	270	LaThuile	MODIS
US-Bkg	2005-2006	GRA	1	4	495	LaThuile	MODIS
US-Blo	2000-2006	ENF	4.7	12.5	1315	FLUXNET2015	Copernicus
US-Bo1	1997-2006	CRO	3	10	217	LaThuile	MODIS
US-Cop	2002-2003	GRA	0.5	1.85	1520	FLUXNET2015	Copernicus
US-FPe	2000-2006	GRA	0.3	3.5	638	LaThuile	MODIS
US-GLE	2009-2014	ENF	10	23	3197	FLUXNET2015	Copernicus
US-Goo	2004-2006	GRA	0.3	4	87	LaThuile	MODIS
US-Ha1	1992-2012	DBF	25	30	340	FLUXNET2015	MODIS
US-Ho1	1996-2004	ENF	20	29	72	LaThuile	MODIS
US-KS2	2003-2006	CSH	2	3.5	3	FLUXNET2015	MODIS
US-Los	2000-2008	WET	2	10.2	480	FLUXNET2015	MODIS
US-Me2	2002-2014	ENF	16	29	1253	FLUXNET2015	Copernicus
US-Me4	1996-2000	ENF	20	47	922	LaThuile	MODIS
US-Me6	2011-2014	ENF	5.2	14	998	FLUXNET2015	MODIS
US-MMS	1999-2014	DBF	27	48	275	FLUXNET2015	MODIS
US-MOz	2005-2006	DBF	24	30	212	LaThuile	MODIS
US-Myb	2011-2014	WET	1	3.3	-1	FLUXNET2015	MODIS
US-Ne1	2002-2012	CRO	3	6	361	FLUXNET2015	MODIS
US-Ne2	2002-2012	CRO	2.5	6	362	FLUXNET2015	MODIS
US-Ne3	2002-2012	CRO	2.5	6	363	FLUXNET2015	MODIS
US-NR1	1999-2014	ENF	12	26	3050	FLUXNET2015	MODIS
US-PFa	1995-2014	MF	30	122	470	FLUXNET2015	MODIS
US-Prr	2011-2013	ENF	7	16	210	FLUXNET2015	MODIS
US-SP1	2005	ENF	22	30	47	LaThuile	Copernicus

US-SP2	2000-2004	ENF	1	7	46	LaThuile	Copernicus
US-SP3	1999-2004	EBF	10	15	36	LaThuile	Copernicus
US-SRG	2009-2014	GRA	1	3.25	1291	FLUXNET2015	MODIS
US-SRM	2004-2014	WSA	2.5	6.4	1120	FLUXNET2015	MODIS
US-Syv	2002-2008	MF	27	36	540	FLUXNET2015	MODIS
US-Ton	2001-2014	WSA	7.1	23	177	FLUXNET2015	MODIS
US-Tw4	2014	Wet	0.5	3	-5	FLUXNET2015	Copernicus
US-Twt	2010-2014	CRO	0.5	3.25	-7	FLUXNET2015	Copernicus
US-UMB	2000-2014	DBF	20	50	234	FLUXNET2015	MODIS
US-Var	2001-2014	GRA	0.55	3	129	FLUXNET2015	MODIS
US-WCr	1999-2006	DBF	24	30	520	FLUXNET2015	Copernicus
US-Whs	2008-2014	OSH	0.5	4	1370	FLUXNET2015	MODIS
US-Wkg	2005-2014	GRA	1	6.4	1531	FLUXNET2015	MODIS
ZA-Kru	2000-2002	SAV	12	16	359	FLUXNET2015	MODIS
ZM-Mon	2008	DBF	12	33	1053	FLUXNET2015	MODIS

Table S3: Participating models. Land surface models that are developed as part of a coupled modelling system are denoted as 'climate' or 'weather' in their Notes, depending on their default application being climate projection or weather forecasting, despite simulations in this experiment being uncoupled/offline. In each case, leaf area index (LAI) is either prescribed, computed by the model itself, or not used (NA).

Model	Institution	LAI	Notes	Authors	References
BEPS	LBL, USA	Prescribed	Ecosystem model; v4.01 (https://github.com/JChen-UToronto/BEPS_hourly_site_4.02)	XL	Liu et al. (1997)
CABLE	UNSW Sydney / CLEX, Australia	Prescribed	Land surface model, climate; r8002; biophysics only, no C-N-P.	MdK, AU	Kowalczyk et al. (2006); Wang et al. (2011)
CABLE-POP	UWS / CSIRO, Australia	Prescribed	Land surface model, offline only. C-N cycle included.	JK	Haverd et al. (2013; 2016; 2018)
CHTESSEL (currently ECLand)	ECMWF, UK	Prescribed	Land surface model, weather. 3 simulation sets, forced locally and with ERA5.	DF, SB, GB	van den Hurk et al. (2000); Balsamo et al. (2009); Dutra et al. (2010); Boussetta et al. (2013)
CLM	NCAR, USA	Prescribed	Land surface model, climate; v5.0.34	KO, DL	Lawrence et al. (2019)
ORCHIDEE2	LSCE/IPSL	Computed	Land surface model, climate and CO_2 forcing. Model version used in CMIP6 (no C-N)	XW-F, CO, PP, NV	Krinner et al. (2005),

ORCHIDEE3	LSCE/IPSL	Computed	Model version based on ORC2 but with Nitrogen cycle and C-N interactions	XW-F, CO,PP, NV	Vuichard et al.,(2019)
JULES	Met Office, UK	Prescribed	Land surface model, weather and climate.	HR, MB	Best et al. (2011); Clark et al. (2011)
Manabe bucket	Met Office, UK	NA	Mechanistic benchmark	MB	Manabe (1969)
Penman Monteith PET	Met Office, UK	NA	Mechanistic benchmark; estimate of potential evapotranspiration (PET)	MB	Monteith & Unsworth (1990)
GFDL	NOAA GFDL, USA	Computed	Land surface model, climate	SM	Dunne et al. (2020); Shevliakova et al. (2023)
MATSIRO	U Tokyo, Japan	Prescribed	Land surface model, climate	TN, HK	MATSIRO6 Document Writing Team (2021)
STEMMUS - SCOPE	U Twente, Netherlands / Northwest Agriculture and Forestry U, China	Prescribed	Land surface model, offline only; R1.3.0 (https://github.com/EcoExtreML/STEMMUS_SCOPE)	YZ, YW, BS	Wang et al. (2021)
EntTBM	Yonsei U, Korea	Prescribed	Ecosystem model within the Earth System Modeling Framework (ESMF), coupled to the NASA Goddard Institute for Space Studies (GISS) GCM ModelE	YK, KC	Kim et al. (2015)
SDGVM	ORNL, USA / University of Sheffield, UK	Computed	Ecosystem model; carbon cycle model (https://bitbucket.org/walkeranthonyp/sdgvm/)	AW	Woodward et al. (1995); Woodward & Lomas (2004); Walker et al. (2017)
LPJ-GUESS	KIT, Germany	Computed	Ecosystem model; v4.0, Lund svn branch plumber, r8913; Qle is based on estimated evaporative demand and modelled soil water supply; Qh estimated from Rnet minus Qle (Note: LWnet component of Rnet and hence Qh during polar night at high latitude (lat > 64) sites is erroneous).	PA	Smith et al. (2014)
MuSICA	INRAE, France	Prescribed	Ecosystem model; Revision 710844c, veg params from Cable-POP, soil texture from soilgrids.org and soil hydraulic params from Montzka et al. (ESSD 2017)	MC, JO	Ogée et al. (2003); Gennaretti et al. (2020)
QUINCY	MPI BGC	Computed	Ecosystem model;	SC, SZ	Thum et al. (2019)
Noah-MP	NASA, U-Albany	Computed	V4.0.1; land surface model included in U.S. National Water Model and U.S. Unified Forecast System; run in NASA-LIS v7.2r (Kumar et al., 2006) ISRIC SoilGrids v2017 250m soil texture (Hengl et al. 2017); Vegetation fraction prescribed as annual maximum of NOAA-NCEP 1985-1989 AVHRR-based monthly climatology	CF	Niu et al. (2011); He et al. (2023)
Empirical: LSTM	University of Alabama	Prescribed	Empirical benchmark; three sites out-of-sample at a time. Two versions created - one to predict raw fluxes and on to predict energy-balance corrected fluxes	CB, JF, GN	

| Empirical: RF | UNSW Sydney / CLEX Australia | Prescribed | Empirical benchmark; one site out-of-sample at a time. Two versions created - one to predict raw fluxes and on to predict energy-balance corrected fluxes. | SH, GA | |
| Empirical: clustering & regression | UNSW Sydney / CLEX Australia | NA | Empirical benchmark; one site out-of-sample at a time. Two versions created of 1lin and 3km27 - one to predict raw fluxes and on to predict energy-balance corrected fluxes | JCP, GA | Abramowitz (2012), Haughton et al. (2018) |

Table S4: The independent set of metrics used to assess aggregate performance. Metrics are calculated on all time steps (*i=1,..,n*) of observations (O) and each model (M) separately for each site. *B* is the number of bins used for density estimation, in this case 2048.

Mean Bias Error (MBE)	$\dfrac{\sum_{i=1}^{n}(M_i - O_i)}{n}$
Standard Deviation (SD)	$\left\| 1 - \dfrac{\sqrt{\frac{\sum_{i=1}^{n}(M_i - \bar{M})^2}{n-1}}}{\sqrt{\frac{\sum_{i=1}^{n}(O_i - \bar{O})^2}{n-1}}} \right\|$
Correlation Coefficient (r)	$1 - \left[\dfrac{n\sum_{i=1}^{n}(O_i M_i) - (\sum_{i=1}^{n}O_i \sum_{i=1}^{n}M_i)}{\sqrt{\left(n\sum_{i=1}^{n}O_i^2 - (\sum_{i=1}^{n}O_i)^2\right)\left(n\sum_{i=1}^{n}M^2{}_i - (\sum_{i=1}^{n}M_i)^2\right)}} \right]$
Normalised Mean Error (NME)	$\dfrac{\sum_{i=1}^{n}\|M_i - O_i\|}{\sum_{i=1}^{n}\|\bar{O}_i - O_i\|}$
5th percentile difference (5th)	$\|M_5 - O_5\|$
95th percentile difference (95th)	$\|M_{95} - O_{95}\|$
Density overlap percentage (PDF)	$100 - \left[\dfrac{range(M,O)}{B} \cdot \left(\sum_{b=1}^{B} min(M_b, O_b)\right) \cdot 100\right]$
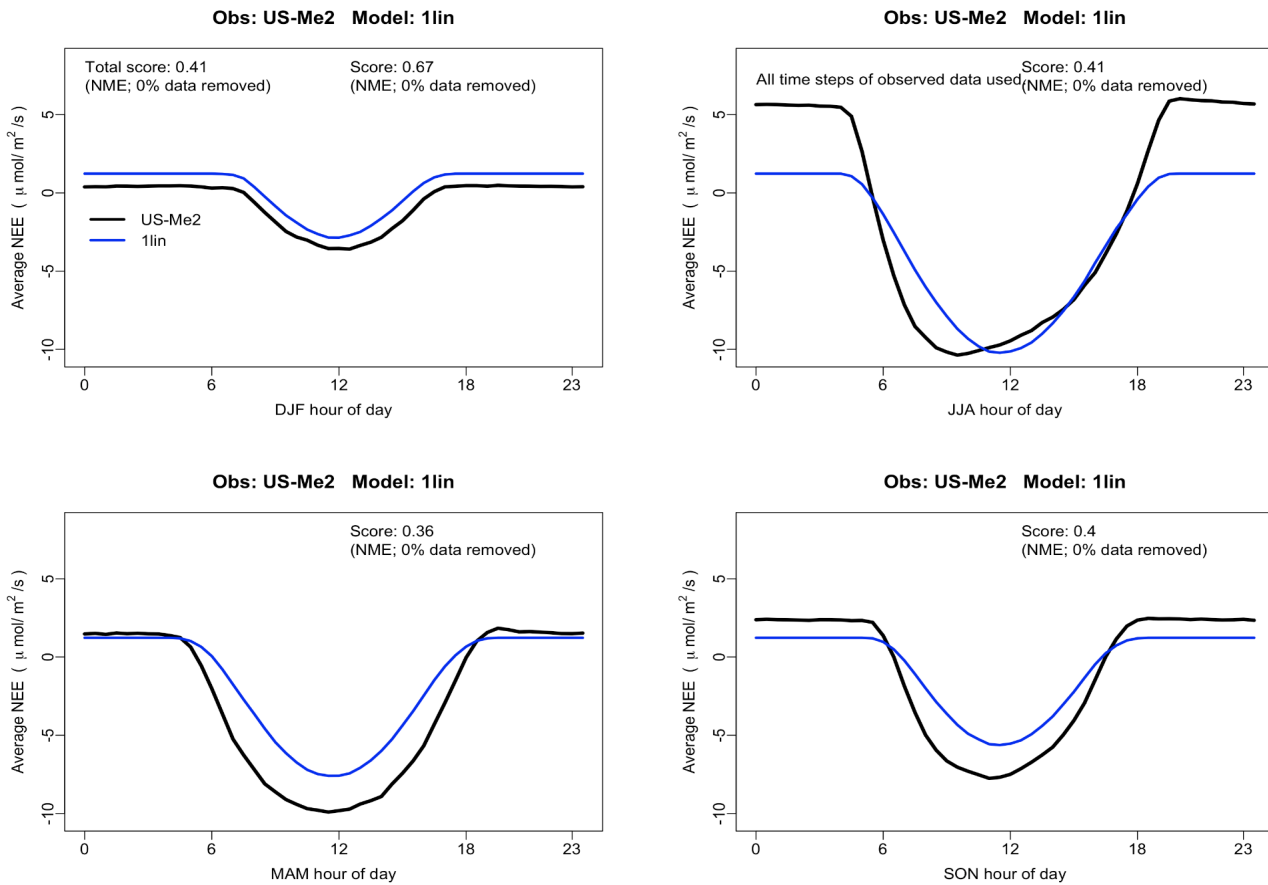
Figure S4: Performance of the 1lin model for the diurnal cycle of Net Ecosystem Exchange of CO₂ (NEE) at the US-Me2 site, with separate panels for each season. This model is an instantaneous linear response to half-hourly SWdown, and no data from this site was used in the training of the regression.
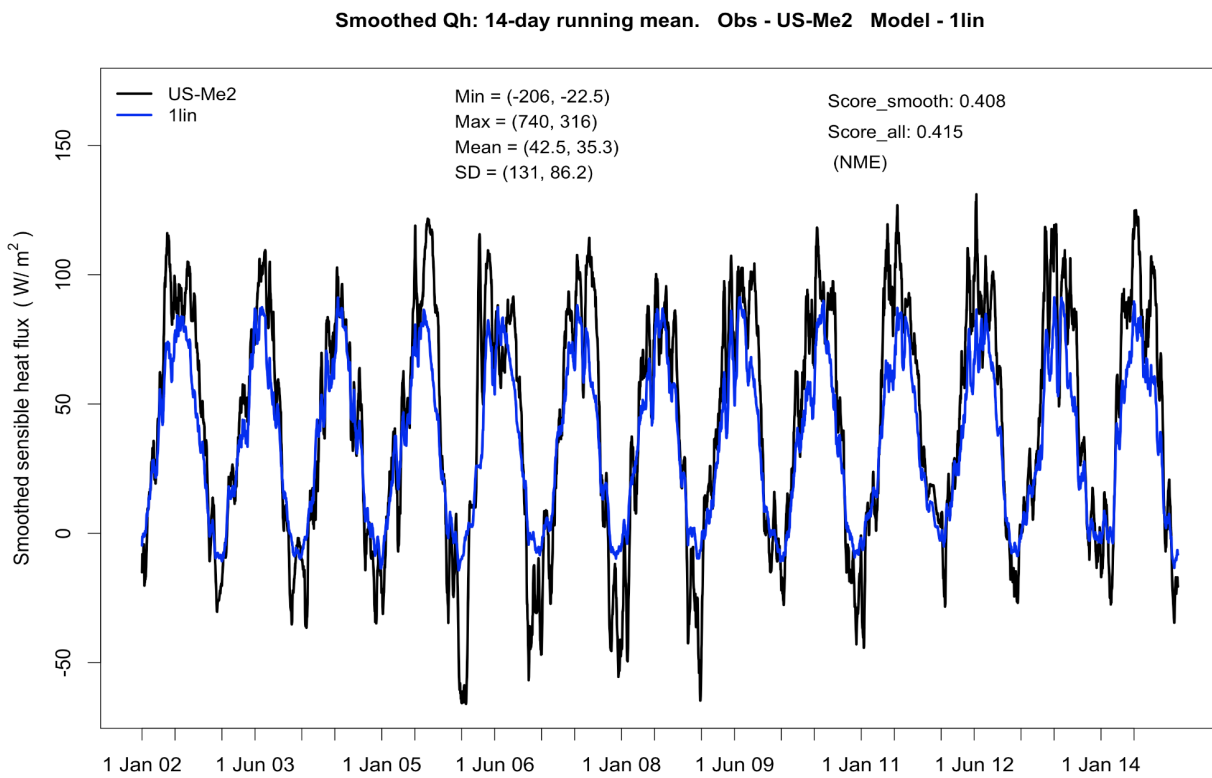
Figure S5: Performance of the 1lin model for a smoothed time series of sensible heat flux (Qh) at the US-Me2 site. This model is an instantaneous linear response to half-hourly SWdown, and no data from this site was used in the training of the regression.

Average monthly Qle: Obs - US-Me2   Model - 1lin

— US-Me2
— 1lin

Score: 0.345
(NME)
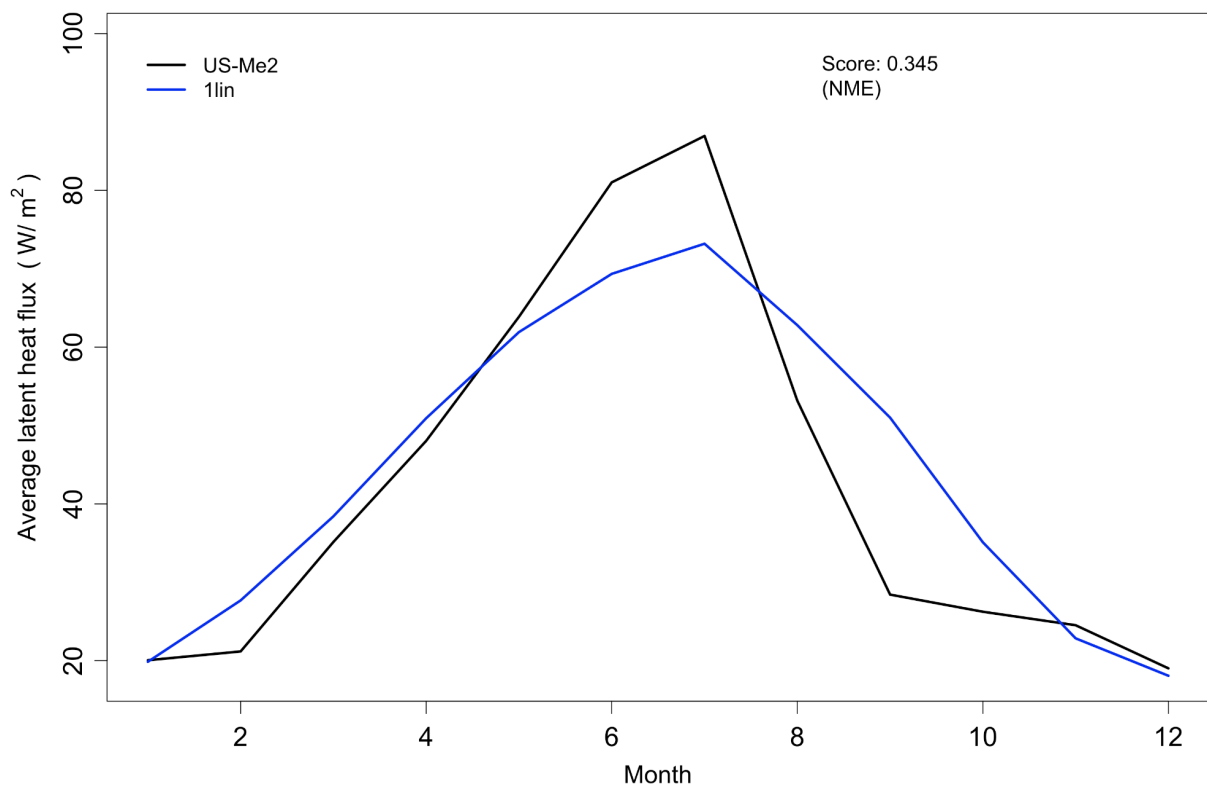
Figure S6: Performance of the 1lin model for average annual cycle of latent heat flux (Qle) at the US-Me2 site. This model is an instantaneous linear response to half-hourly SWdown, and no data from this site was used in the training of the regression.

Average Qle_cor vs Qh_cor over all sites

Legend:
- Obs (# of sites: 154)
- 1lin_raw (154)
- 1lin_eb (154)
- 2lin_raw (154)
- 3km27_raw (154)
- 3km27_eb (154)
- 6km729_raw (154)
- 6km729lag_raw (154)
- RF_raw (154)
- RF_eb (154)
- LSTM_raw (154)
- LSTM_eb (154)
- PenmanMonteith (154)
- Manabe (154)
- CABLE (154)
- CABLE-POP (154)
- CHTESSEL_1 (154)
- CHTESSEL_ERA5_3 (154)
- CHTESSEL_ERA5_4 (154)
- CLM5 (154)
- EntTBM (154)
- GFDL (154)
- JULES_GL9 (154)
- JULES_GL9_LAI (154)
- LPJ-GUESS (146)
- MATSIRO (154)
- MuSICA (154)
- NoahMP (154)
- ORCHIDEE2 (152)
- ORCHIDEE3 (150)
- QUINCY (153)
- STEMMUS-SCOPE (154)

Obs available energy (85 W/m2)
Obs Bowen ratio (0.73)

Figure S7a: Same as Fig. 1, but showing observational crosshair location using energy-balance corrected Qle and Qh using the Fluxnet2015 correction algorithm.

Average Qle vs Qh over all sites

Legend:
- Obs (# of sites: 154)
- 1lin_raw (154)
- 1lin_eb (154)
- 2lin_raw (154)
- 3km27_raw (154)
- 3km27_eb (154)
- 6km729_raw (154)
- 6km729lag_raw (154)
- RF_raw (154)
- RF_eb (154)
- LSTM_raw (154)
- LSTM_eb (154)
- PenmanMonteith (154)
- Manabe (154)
- CABLE (154)
- CABLE-POP (154)
- CHTESSEL_1 (154)
- CHTESSEL_ERA5_3 (154)
- CHTESSEL_ERA5_4 (154)
- CLM5 (154)
- EntTBM (154)
- GFDL (154)
- JULES_GL9 (154)
- JULES_GL9_LAI (154)
- LPJ-GUESS (144)
- MATSIRO (154)
- MuSICA (154)
- NoahMP (154)
- ORCHIDEE2 (152)
- ORCHIDEE3 (150)
- QUINCY (153)
- STEMMUS-SCOPE (154)

Obs available energy (95 W/m2)
Obs Bowen ratio (0.76)

**Figure S7b: Same as Fig. 1, using raw fluxes, but showing results filtered for only those time steps with wind speed > 2ms^{-1}, typically daytime flux values. This clearly results in a higher average available energy, and slight increase in observed Bowen ratio.**

Error in mean water evaporative fraction [Qle/Rainf] over sites
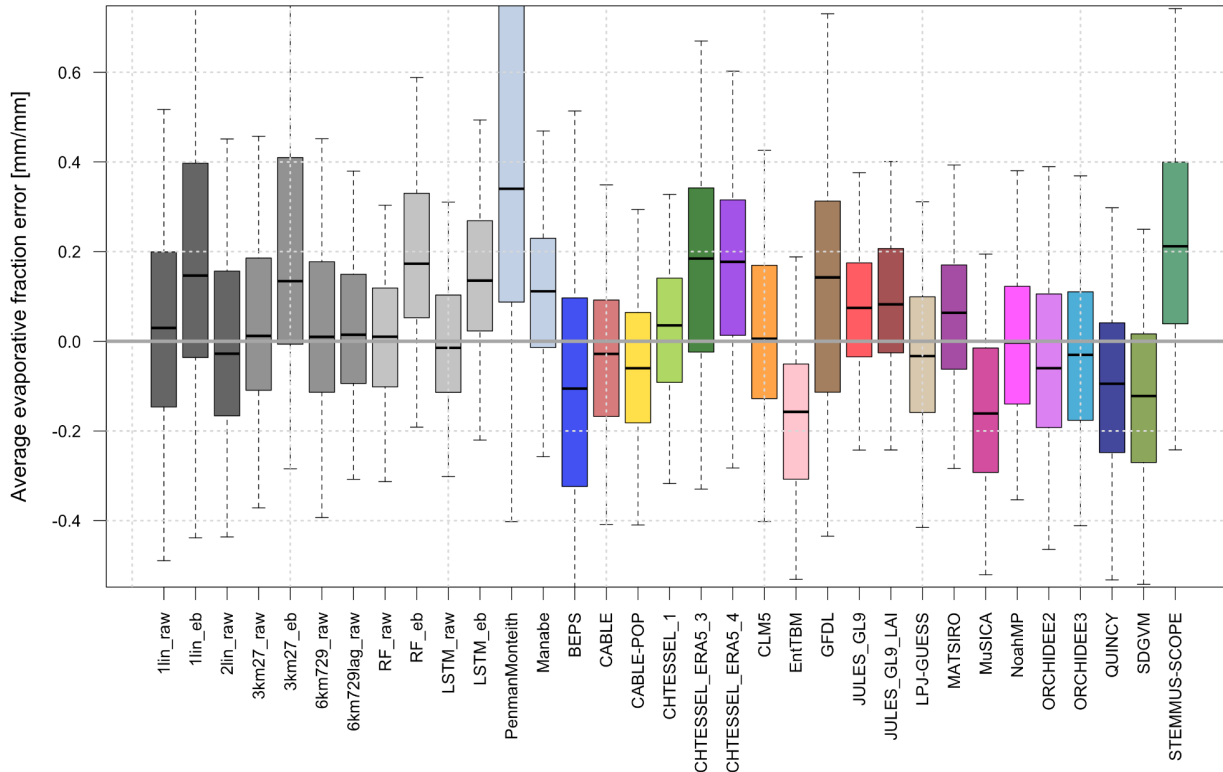
Figure S8a: Mean error in water evaporative fraction (Qle / Rainf), shown as a boxplot across the 154 sites, for each model, using raw flux tower version of Qle.

Error in mean water evaporative fraction [Qle/Rainf] over sites
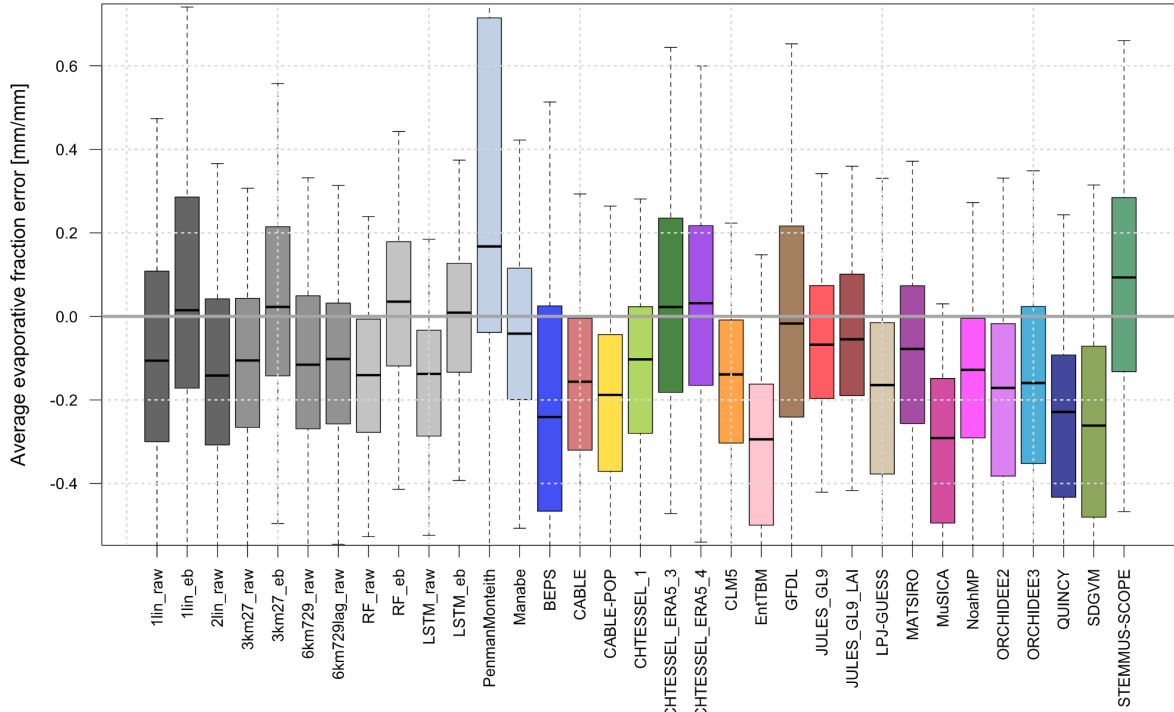
Figure S8b: Mean error in water evaporative fraction (Qle / Rainf), shown as a boxplot across the 154 sites, for each model, using energy-balance corrected version of Qle.

Error in mean water use efficiency over sites [-NEE/Qle]
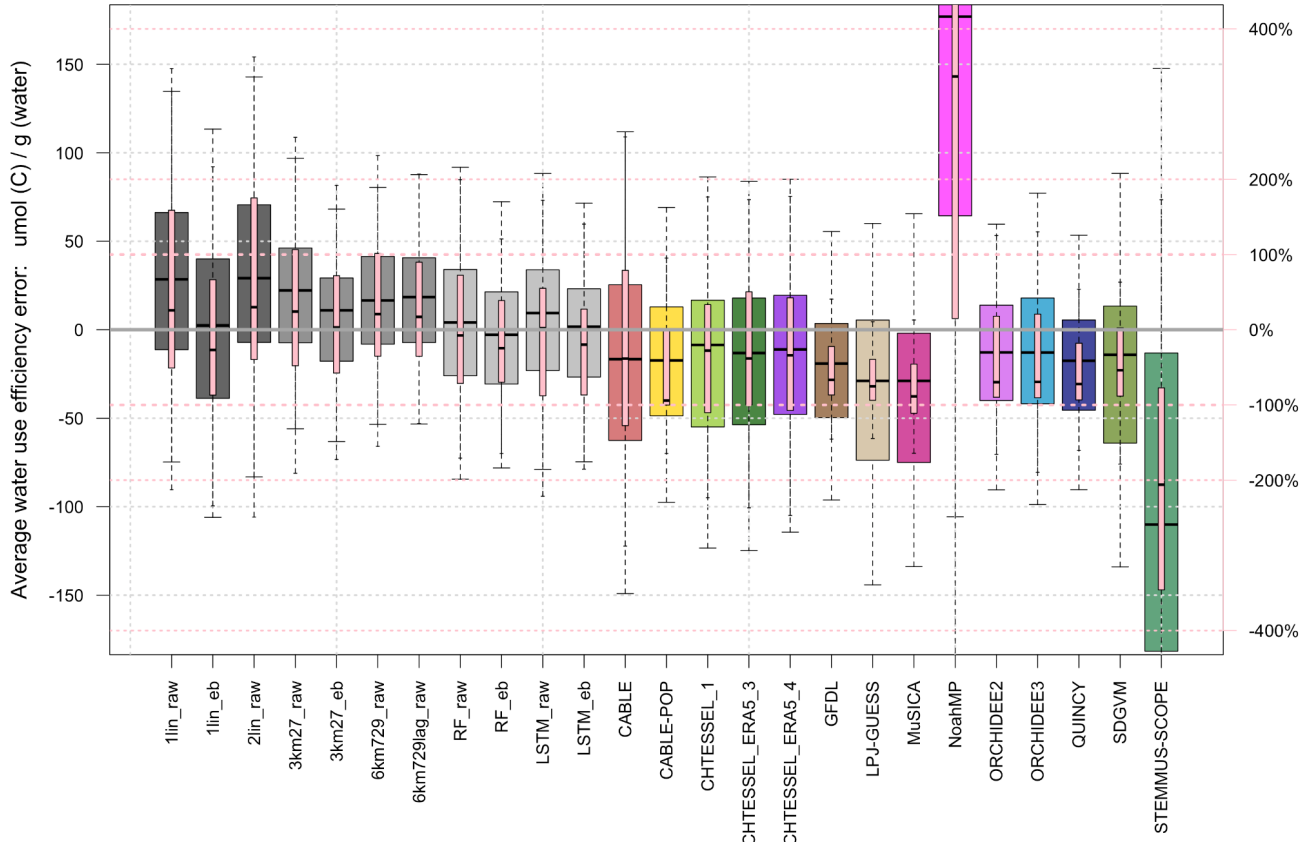
Figure S9: The equivalent of Figure 4, but using the energy balance corrected version of Qle.
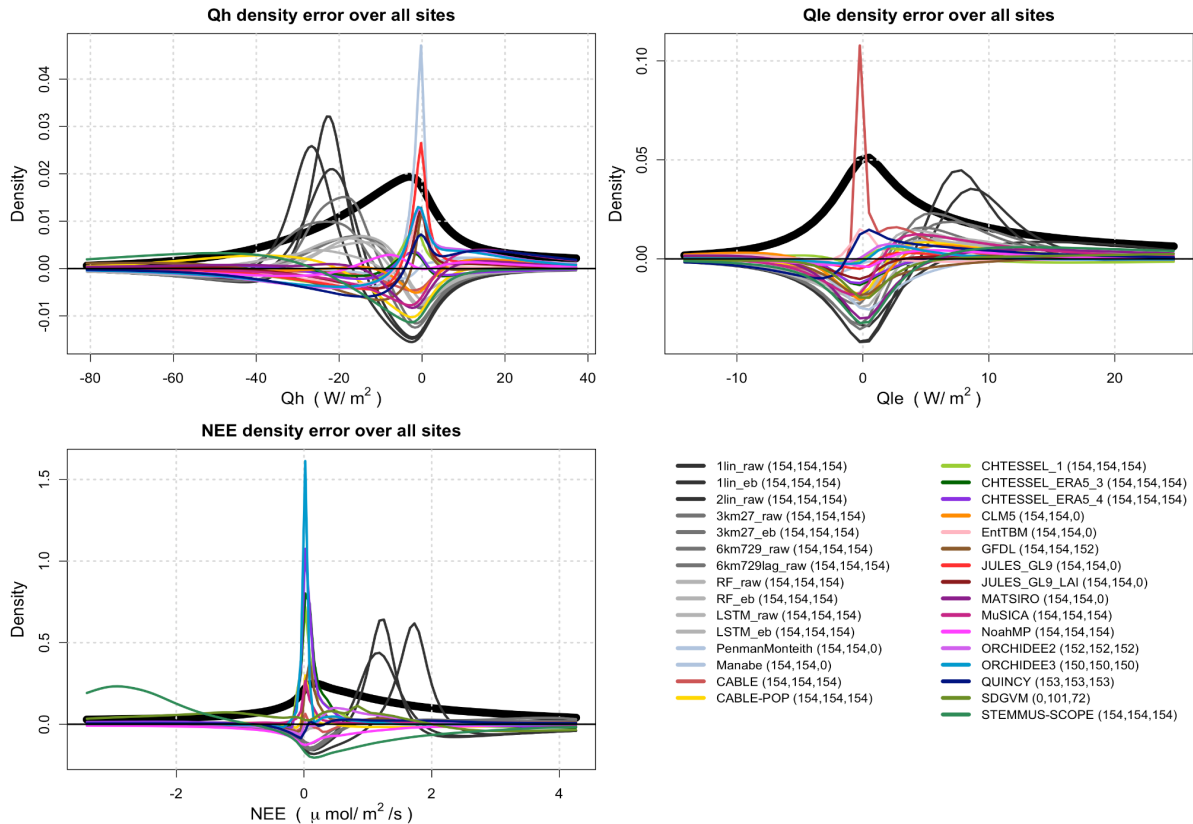
Figure S10a: Error in the density of values of Qle, Qh and NEE relative to observations collated across all sites. The thick black lines show the density of observed values of each variable, and the thinner lines show the modelled density estimate minus the observed density estimate, and so show which magnitudes of fluxes are simulated too often (positive) or not often enough (negative). The vertical axis is the same for both observed density and LM density error. Horizontal axes are restricted to the region of highest density difference.
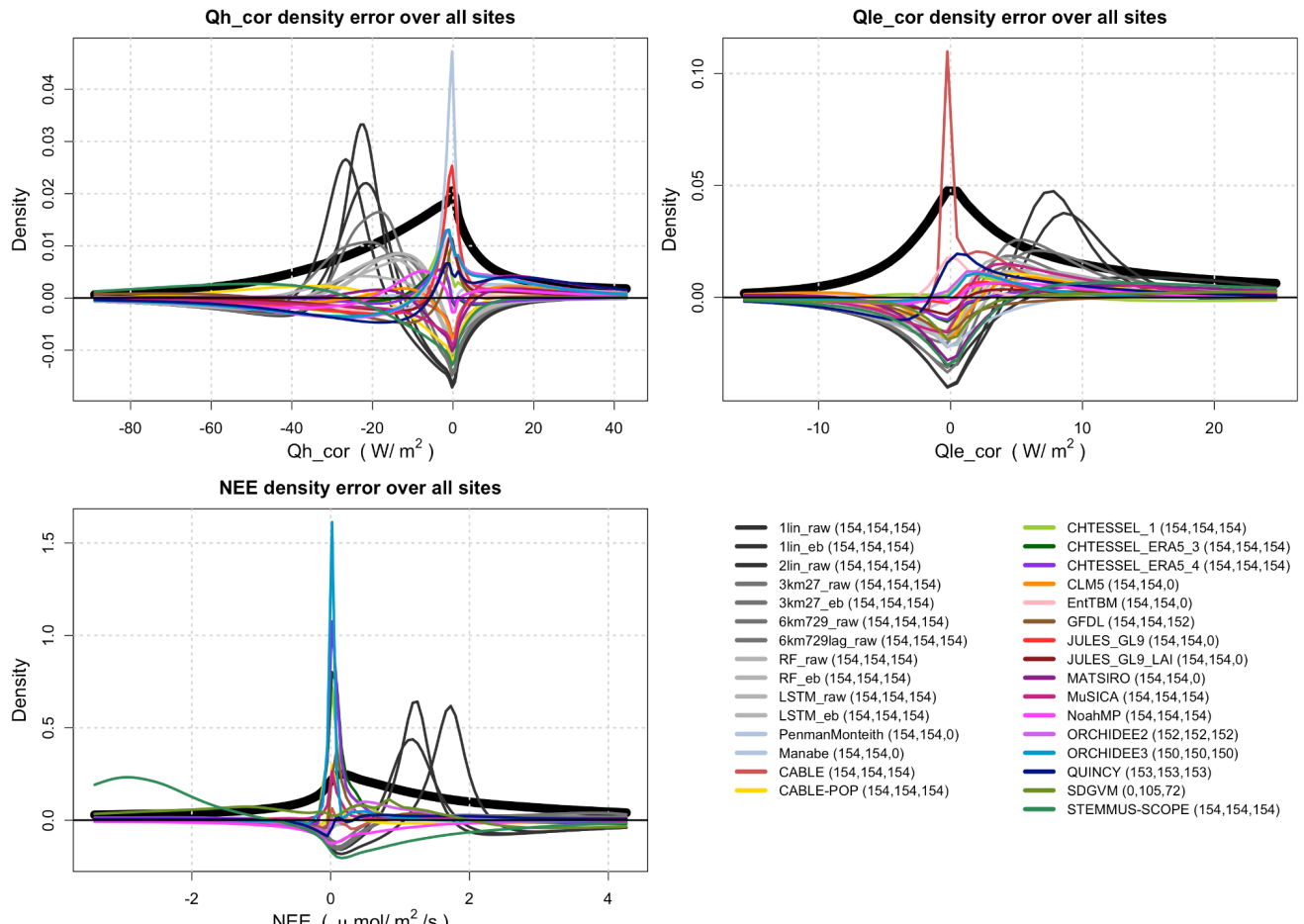
Figure S10b: Same as Figure 4, but using energy balance corrected Qle and Qh fluxes - note that the changes from Figure S10a are remarkably small.
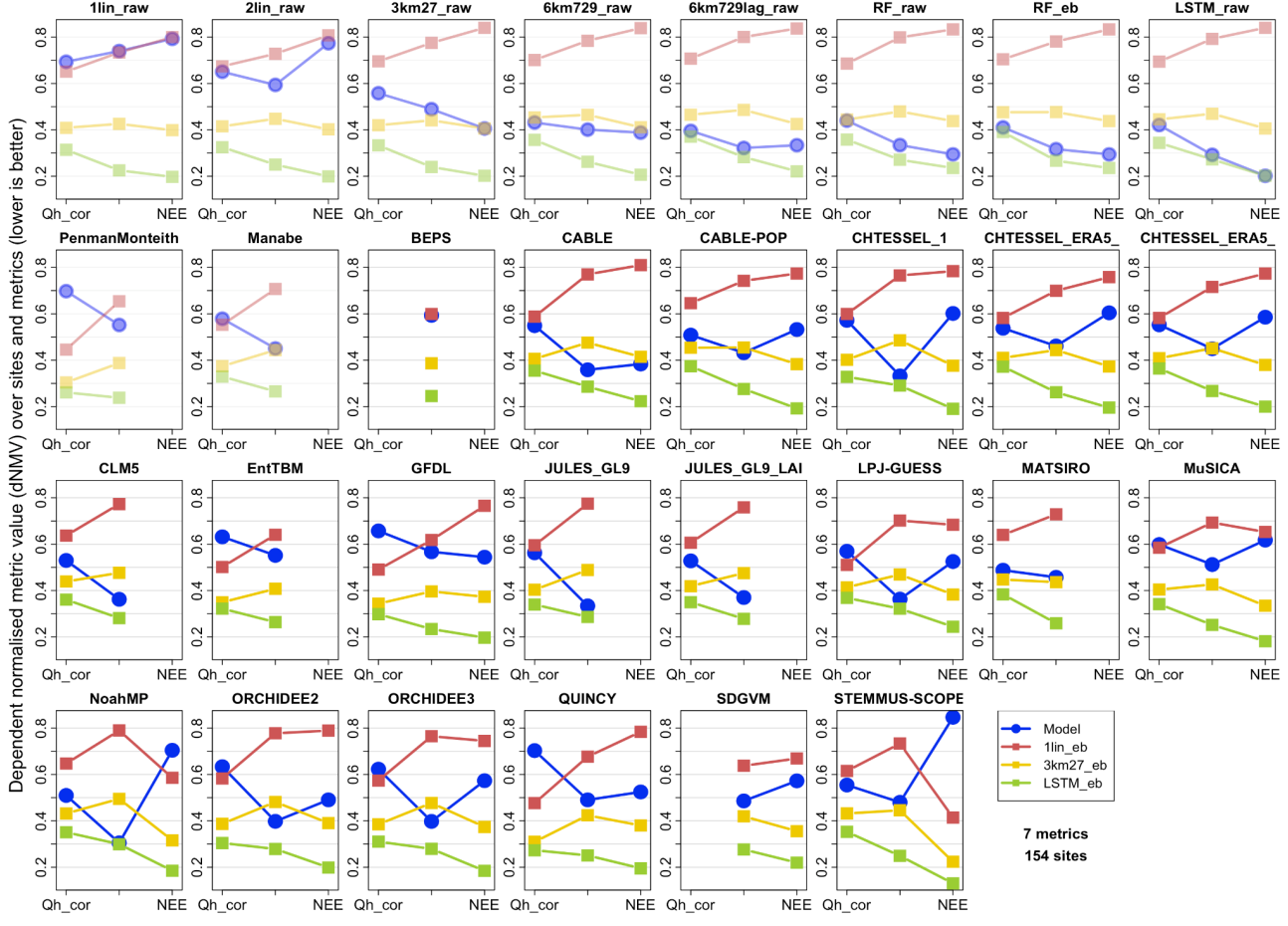
Figure S11a: Same as Fig. 5, showing dNMV, but using the energy-balance corrected observed fluxes for Qle and Qh. Note that the empirical benchmarks used here are those trained to target energy balance corrected fluxes (1lin_eb, 3km27_eb and LSTM_eb).
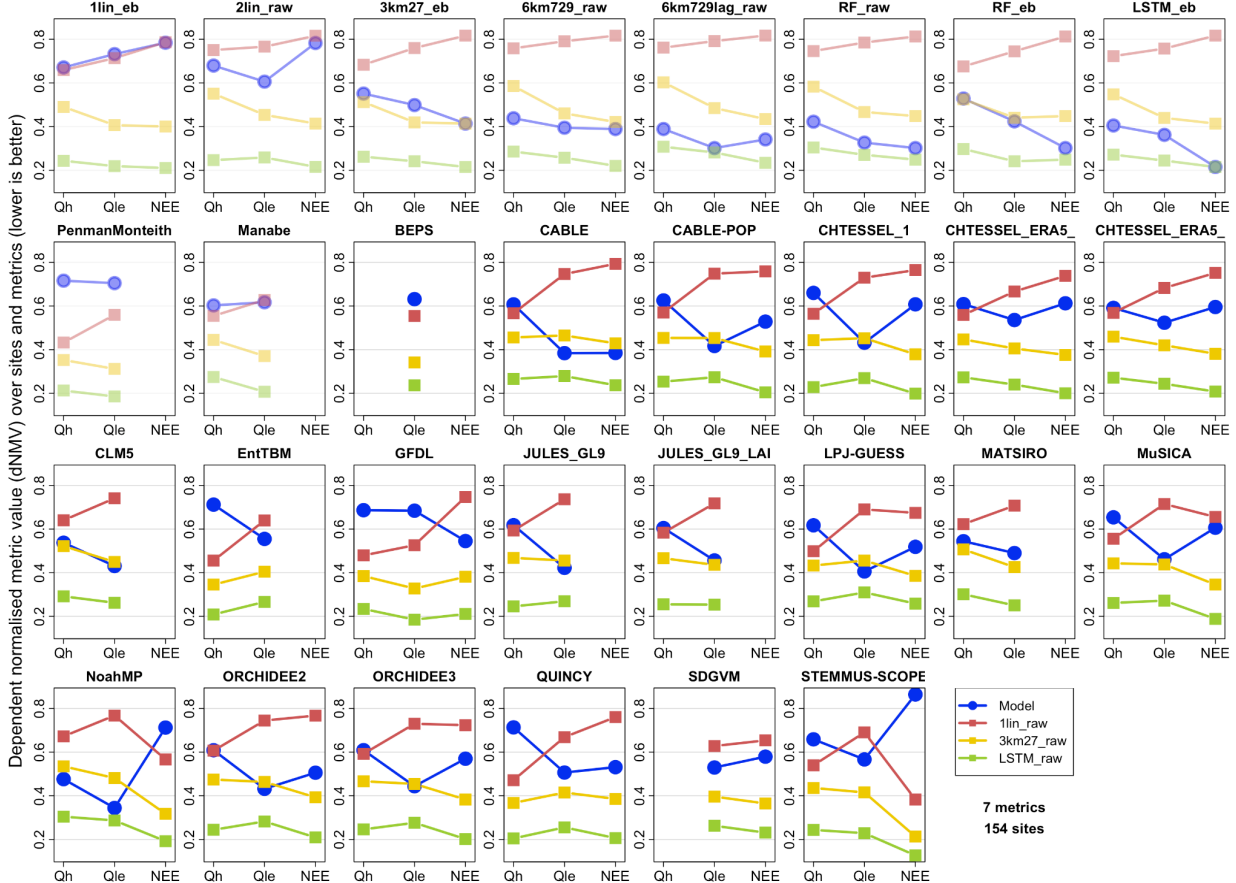
Figure S11b: Same as Figure 5, showing dNMV, using raw fluxes, but showing results filtered for only those time steps with wind speed > 2ms⁻¹, typically daytime flux values.
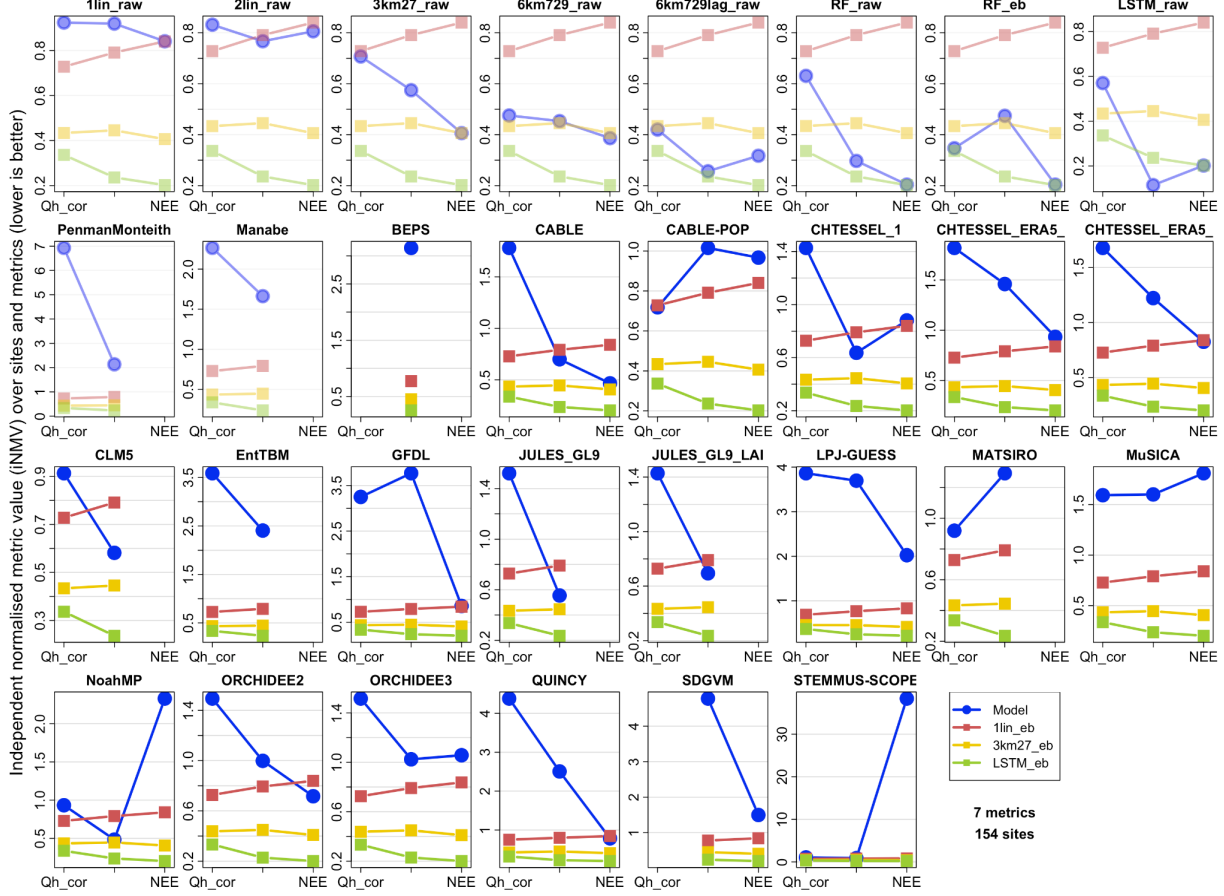
Figure S11c: Same as Figure 5, showing iNMV, but using the energy-balance corrected observed fluxes for Qle and Qh. Note that the empirical benchmarks used here are those trained to target energy balance corrected fluxes (1lin_eb, 3km27_eb and LSTM_eb).
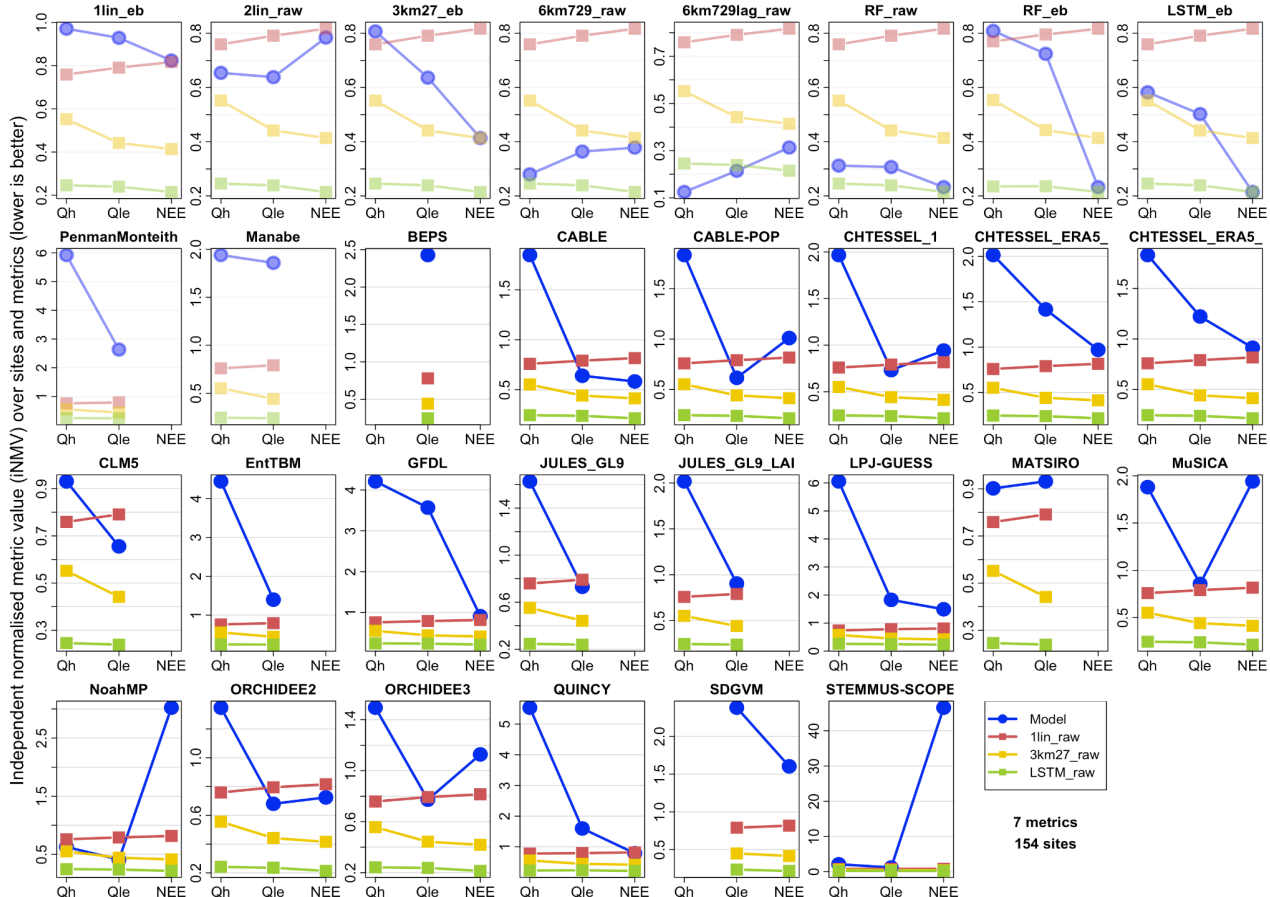
Figure S11d: Same as Figure 6, showing iNMV, using raw fluxes, but showing results filtered for only those time steps with wind speed > 2ms⁻¹, typically daytime flux values.
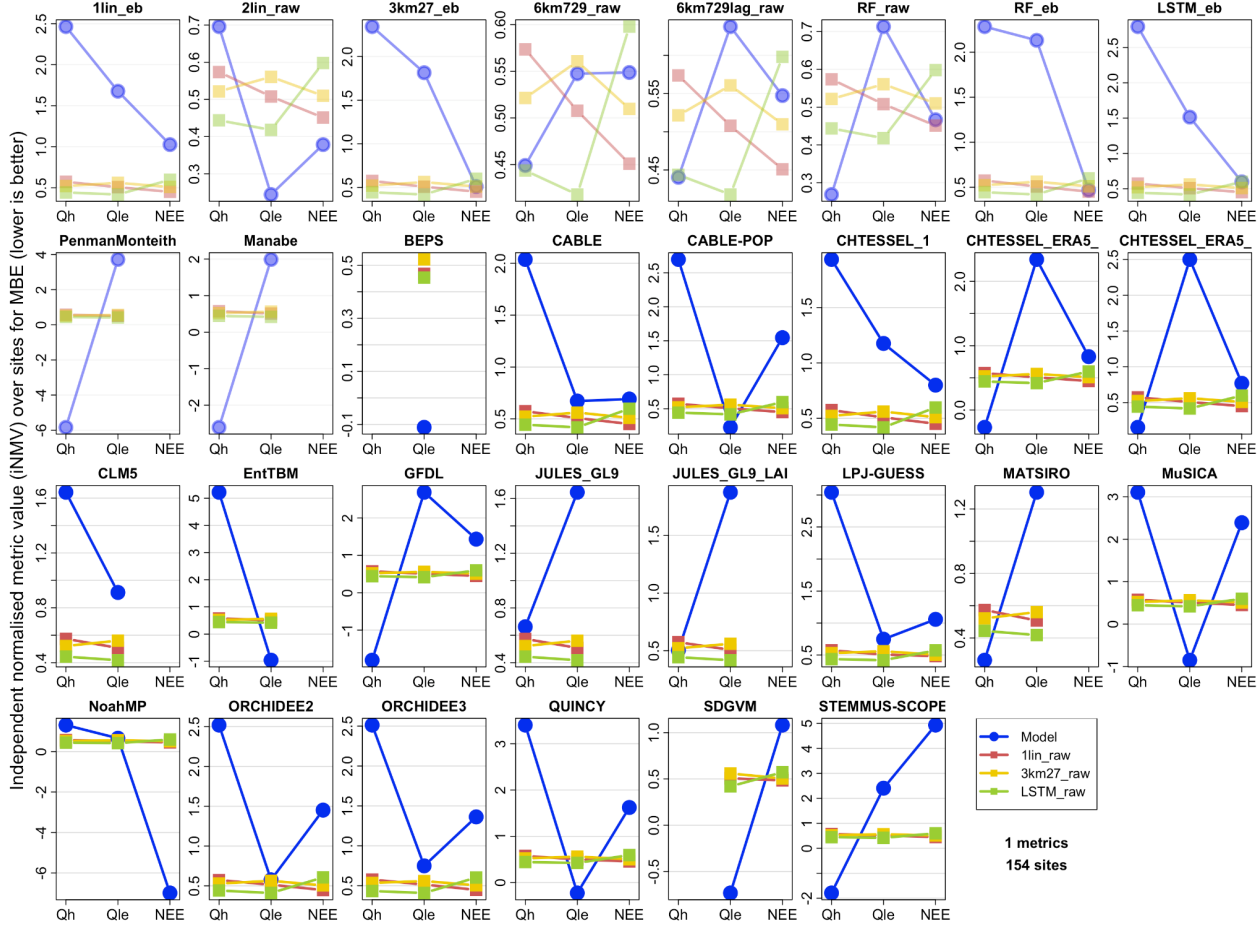
Figure S11e: Same as Figure 6, showing iNMV, using raw fluxes, but showing results only for a single metric in Table S4: Mean Bias Error (MBE).
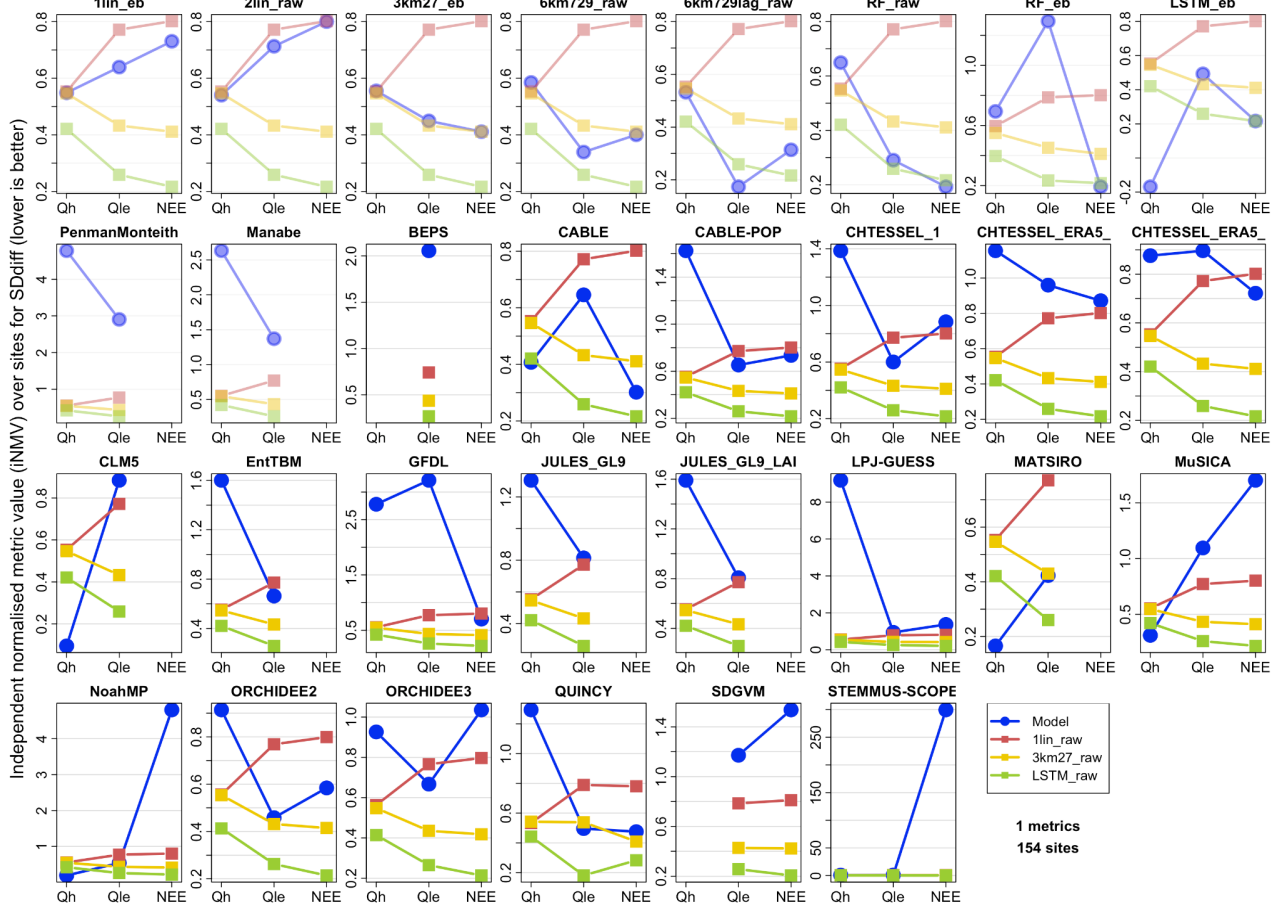
Figure S11f: Same as Figure 6, showing iNMV, using raw fluxes, but showing results only for a single metric in Table S4: Standard Deviation difference (SDdiff).
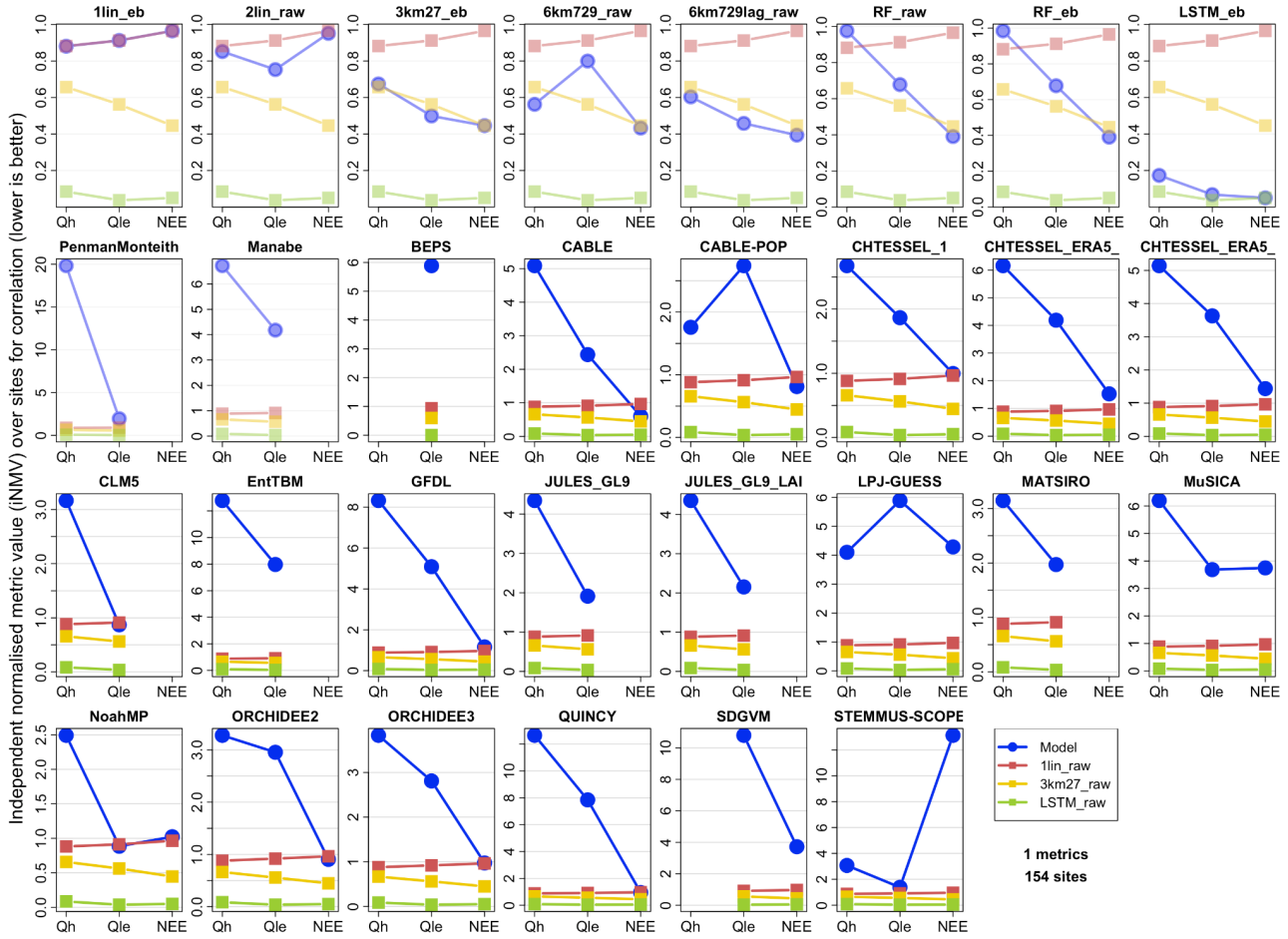
Figure S11g: Same as Figure 6, showing iNMV, using raw fluxes, but showing results only for a single metric in Table S4: Correlation coefficient (r).
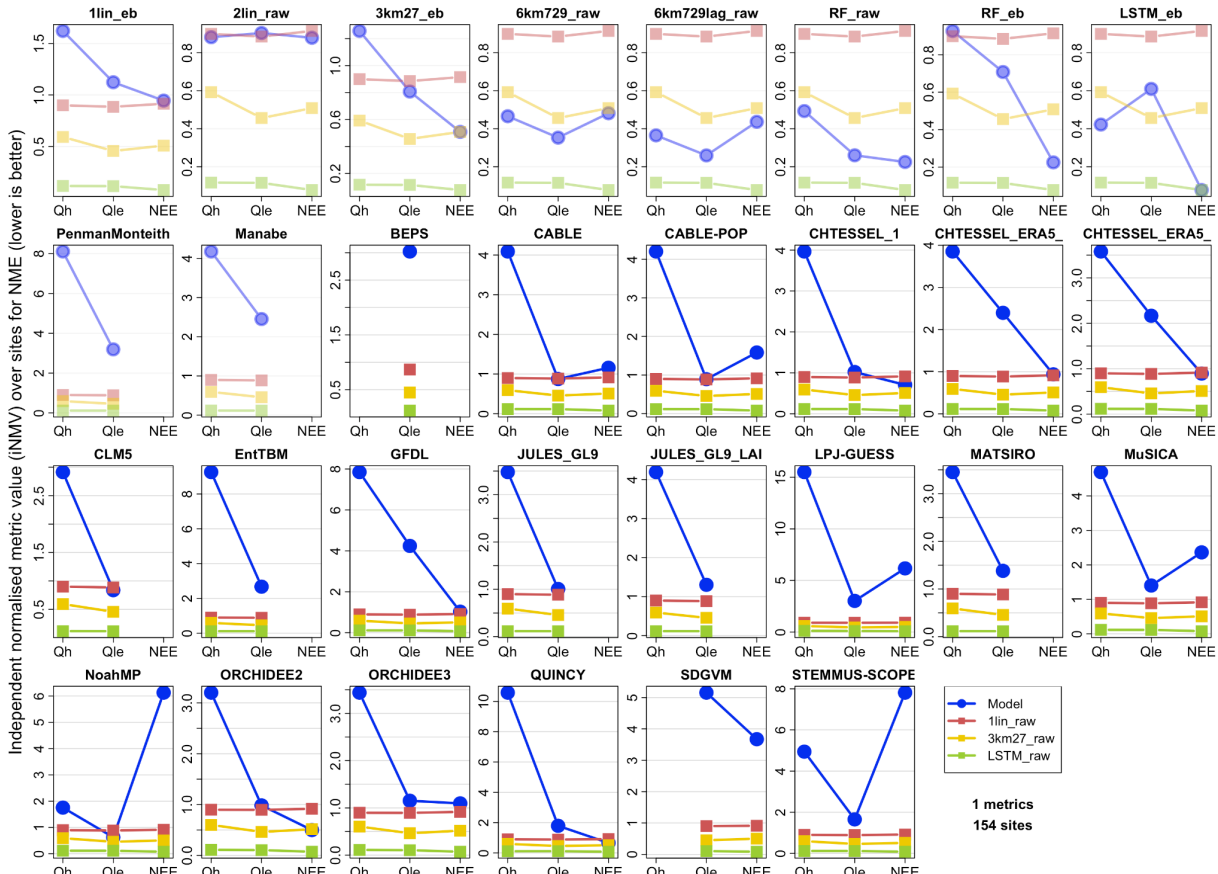
Figure S11h: Same as Figure 6, showing iNMV, using raw fluxes, but showing results only for a single metric in Table S4: Normalised Mean Error (NME).
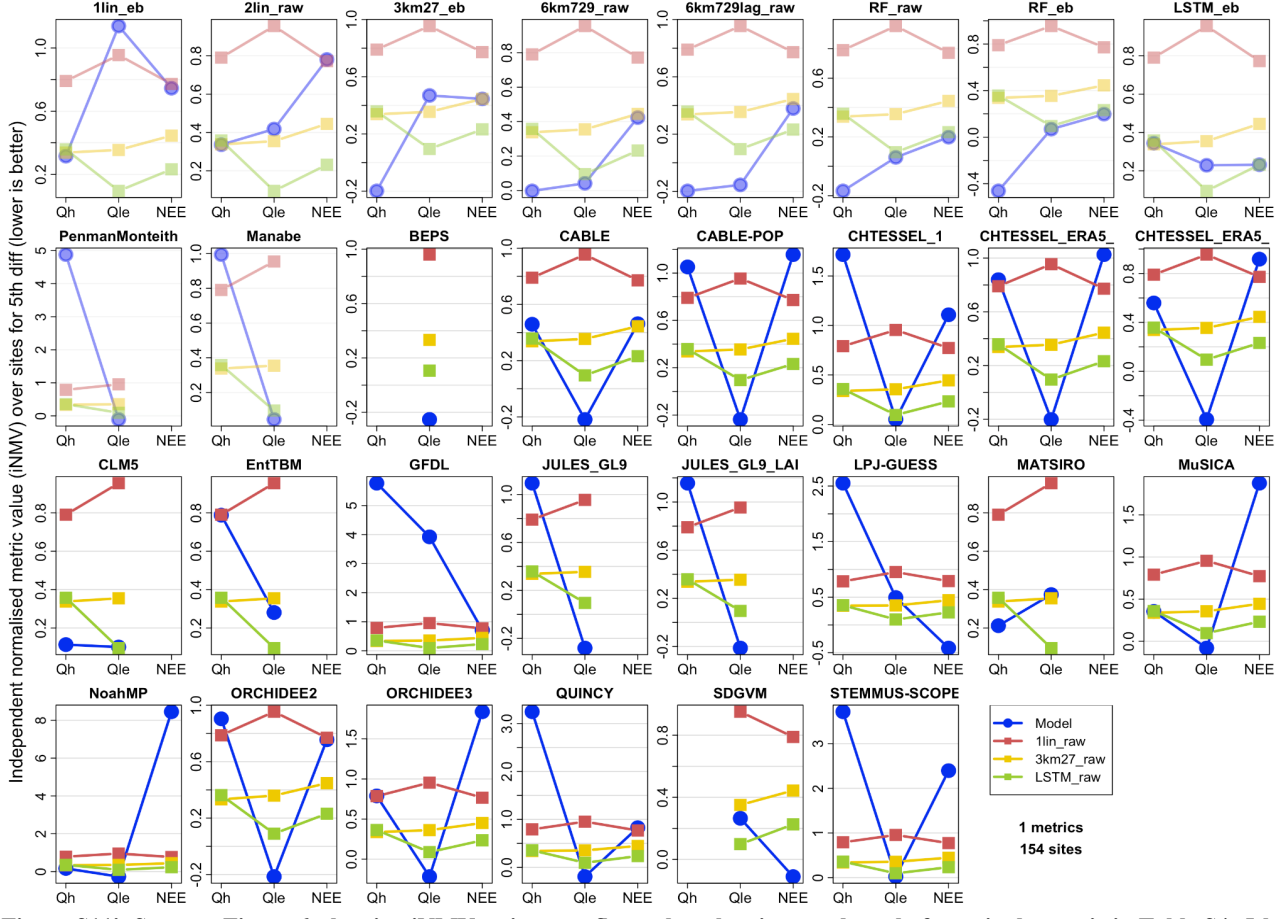
Figure S11i: Same as Figure 6, showing iNMV, using raw fluxes, but showing results only for a single metric in Table S4: 5th percentile difference (5th).
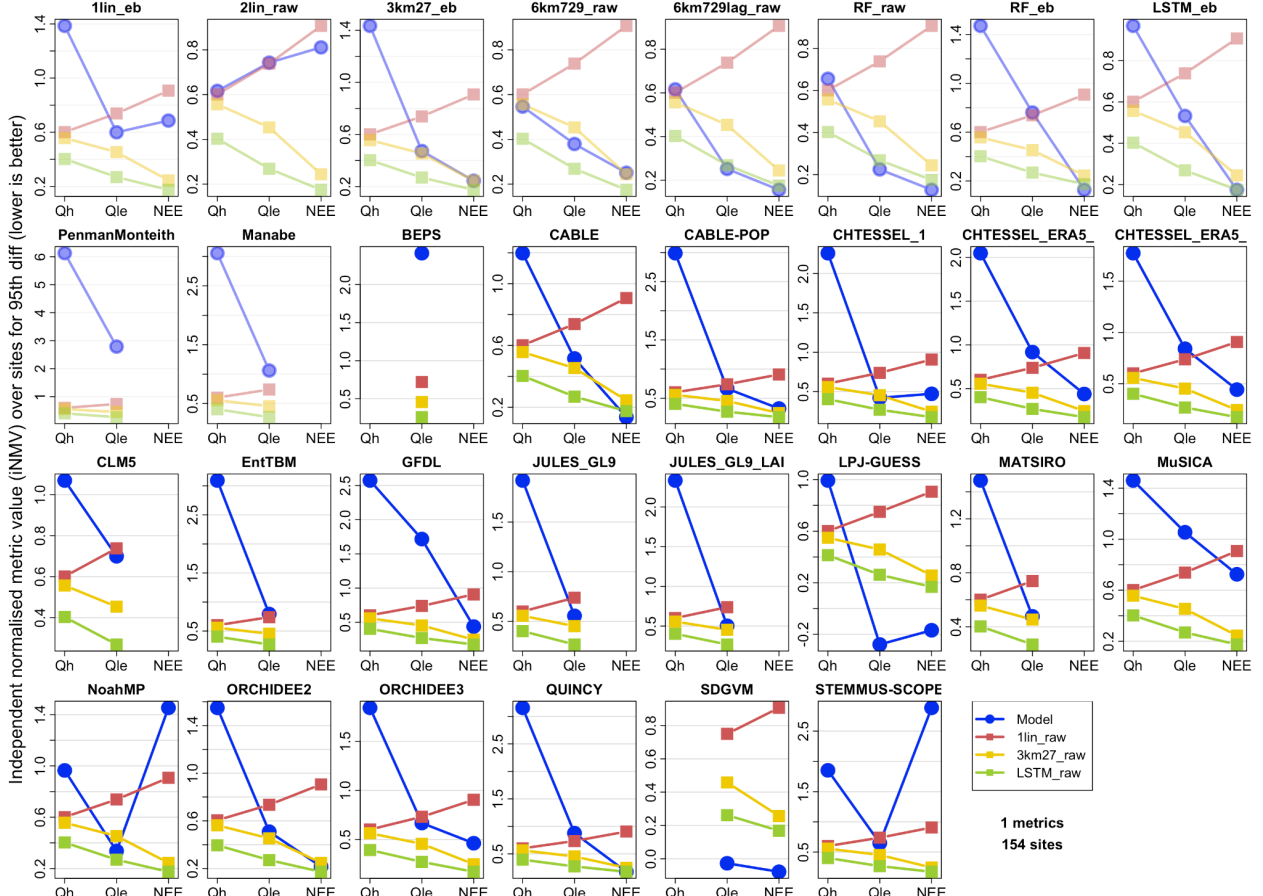
Figure S11j: Same as Figure 6, showing iNMV, using raw fluxes, but showing results only for a single metric in Table S4: 95th percentile difference (95th).
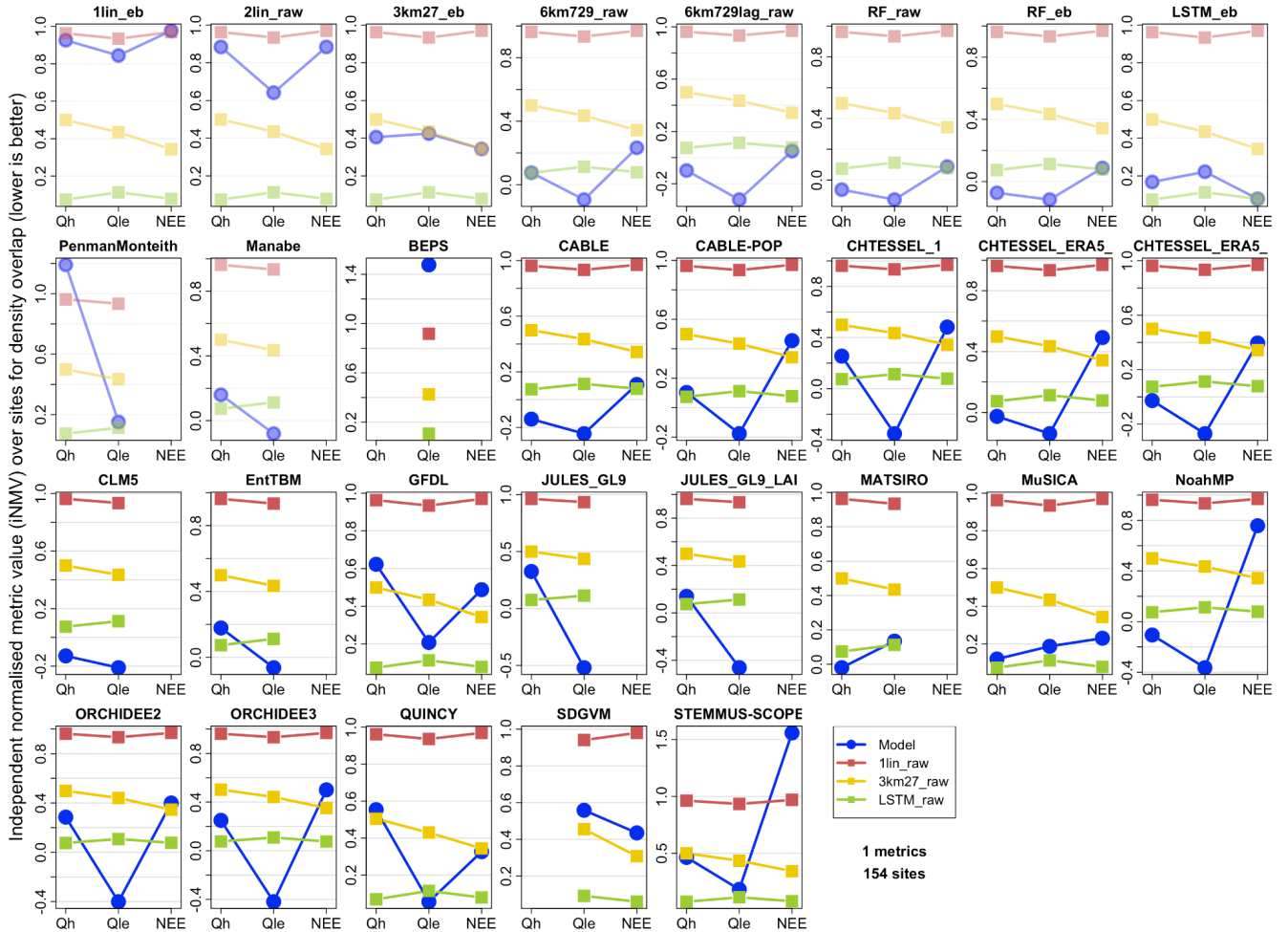
Figure S11k: Same as Figure 6, showing iNMV, using raw fluxes, but showing results only for a single metric in Table S4: Density estimate overlap percentage (PDF).
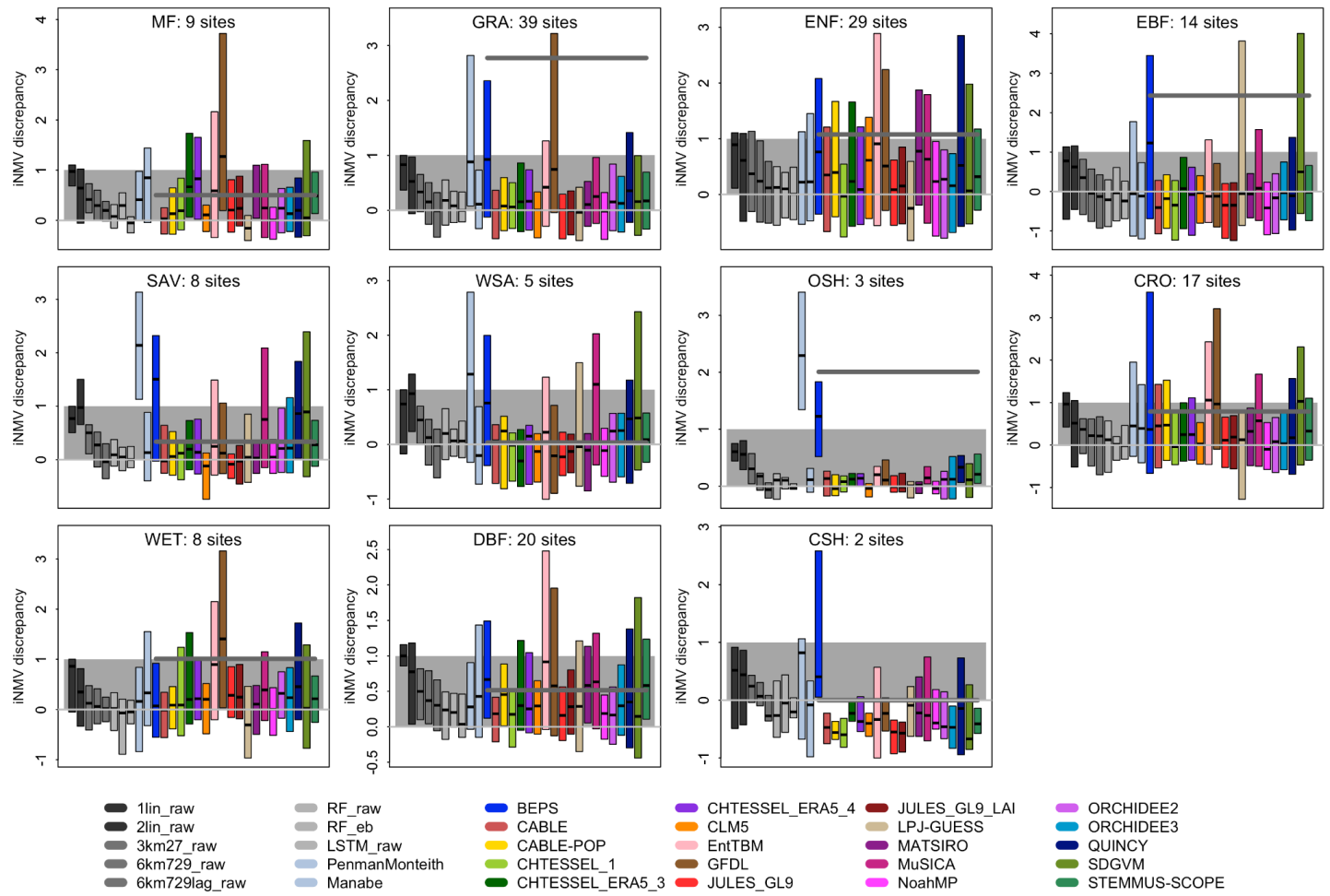
**Figure S12a: Independent normalised metric value (iNMV) discrepancy between each model and LSTM_eb for latent heat flux (Qle), sorted by vegetation type, as per Figure 7, but using energy-balance corrected Qle. The average of all models for each vegetation type is shown by the dark grey bar and the zero line is in light grey, with 0-1 range (grey shading) representing the range of metric values between 1lin and LSTM_eb. Vegetation types are: Mixed Forest (MF); Grassland (GRA); Evergreen Needleleaf (ENF); Evergreen Broadleaf (EBF); Savanna (SAV); Woody Savanna (WSA); Open Shrubland (OSH); Cropland (CRO); Wetland (WET); Deciduous Broadleaf (DBF); Closed Shrubland (CSH).**

# Independent normalised metric value (iNMV) improvement in Qh offered by LSTM_raw
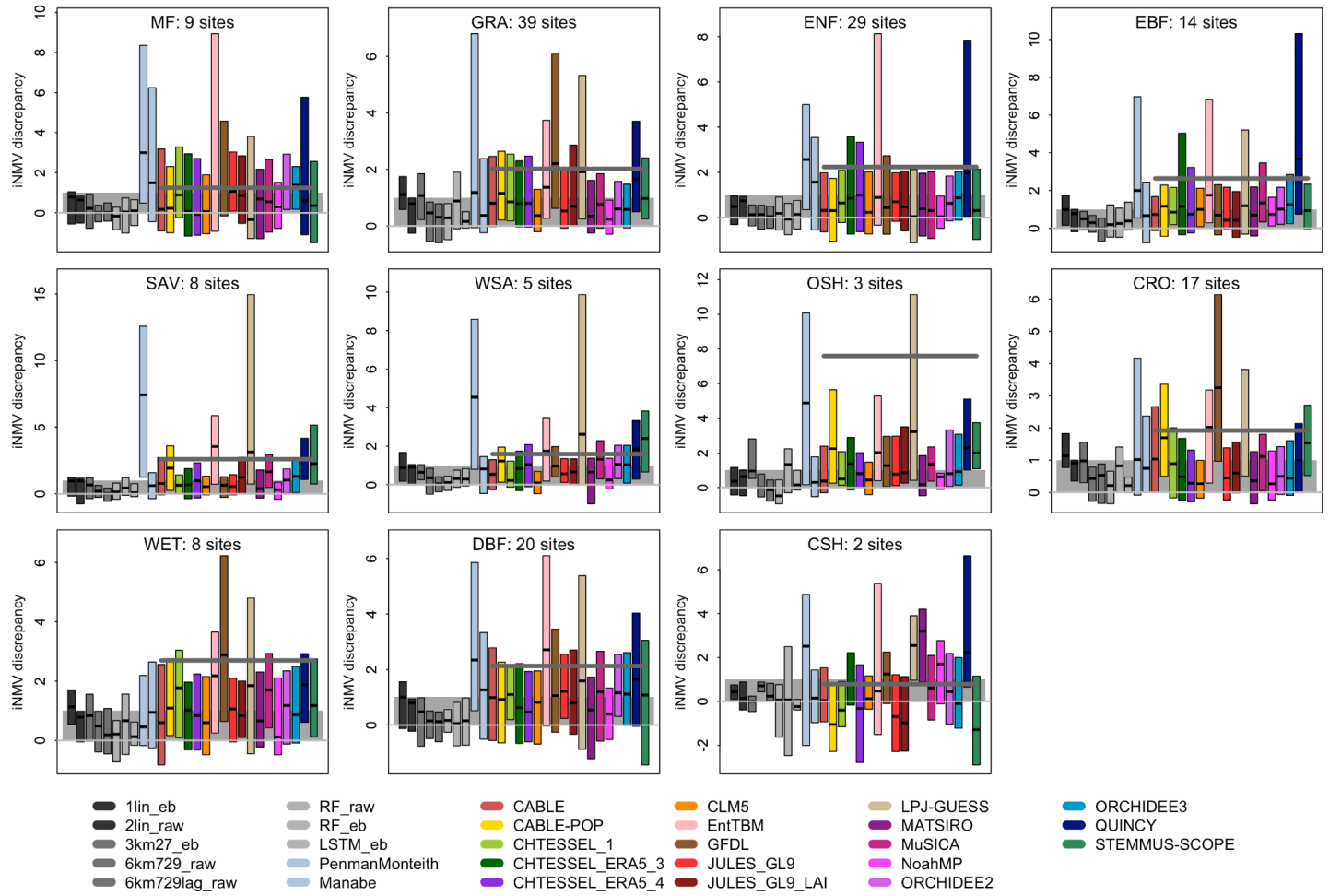
Figure S12b: Independent normalised metric value (iNMV) discrepancy between each model and LSTM_raw for sensible heat flux (Qh), using raw fluxes, sorted by vegetation type, as per Figure 7. Vegetation types are: Mixed Forest (MF); Grassland (GRA); Evergreen Needleleaf (ENF); Evergreen Broadleaf (EBF); Savanna (SAV); Woody Savanna (WSA); Open Shrubland (OSH); Cropland (CRO); Wetland (WET); Deciduous Broadleaf (DBF); Closed Shrubland (CSH).
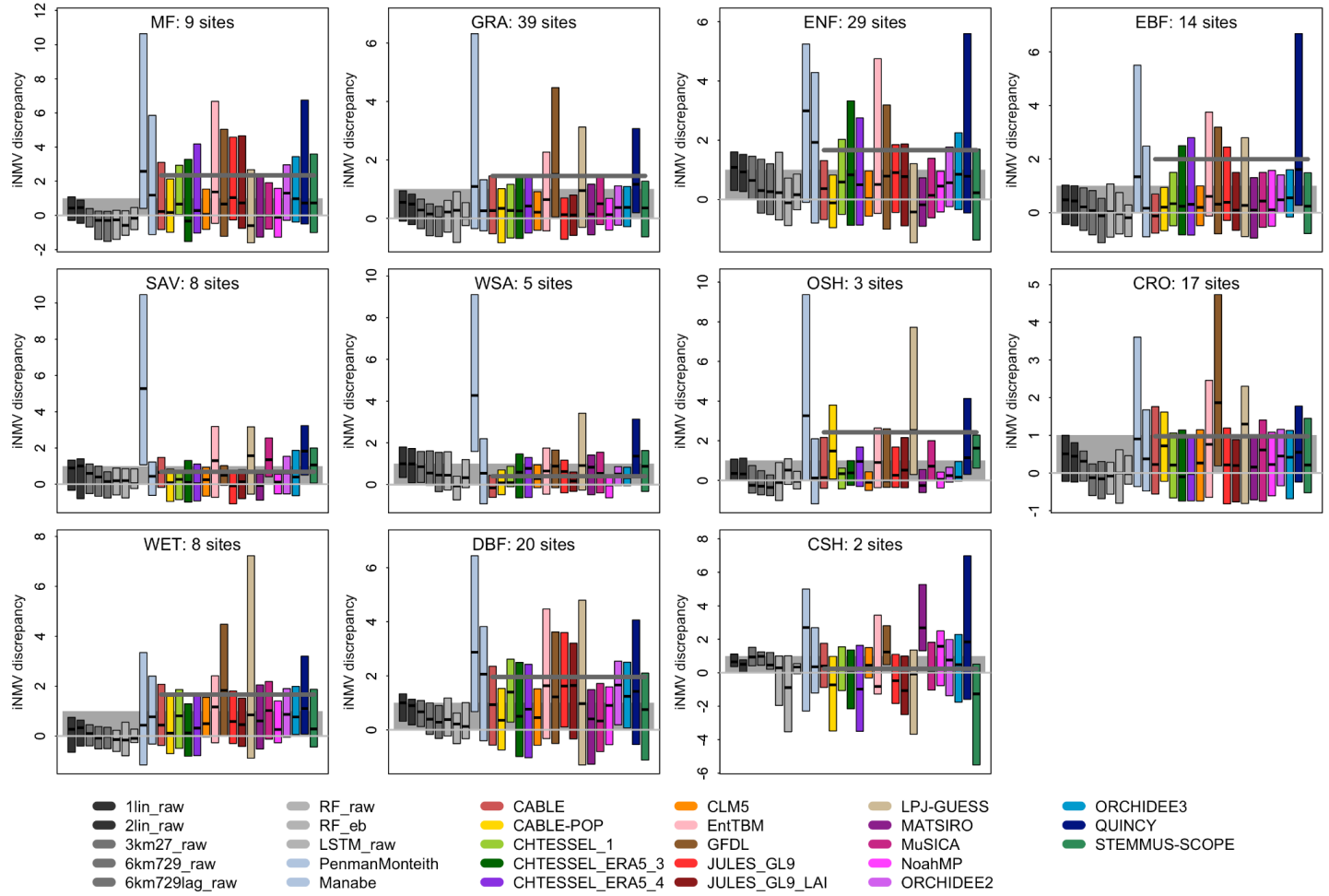
Figure S12c: Normalised metric value (iNMV) discrepancy between each model and LSTM_eb for sensible heat flux (Qh), sorted by vegetation type, as per Figure 7, but using energy-balance corrected Qh, with 0-1 range (grey shading) representing the range of metric values between 1lin and LSTM_eb. Vegetation types are: Mixed Forest (MF); Grassland (GRA); Evergreen Needleleaf (ENF); Evergreen Broadleaf (EBF); Savanna (SAV); Woody Savanna (WSA); Open Shrubland (OSH); Cropland (CRO); Wetland (WET); Deciduous Broadleaf (DBF); Closed Shrubland (CSH).
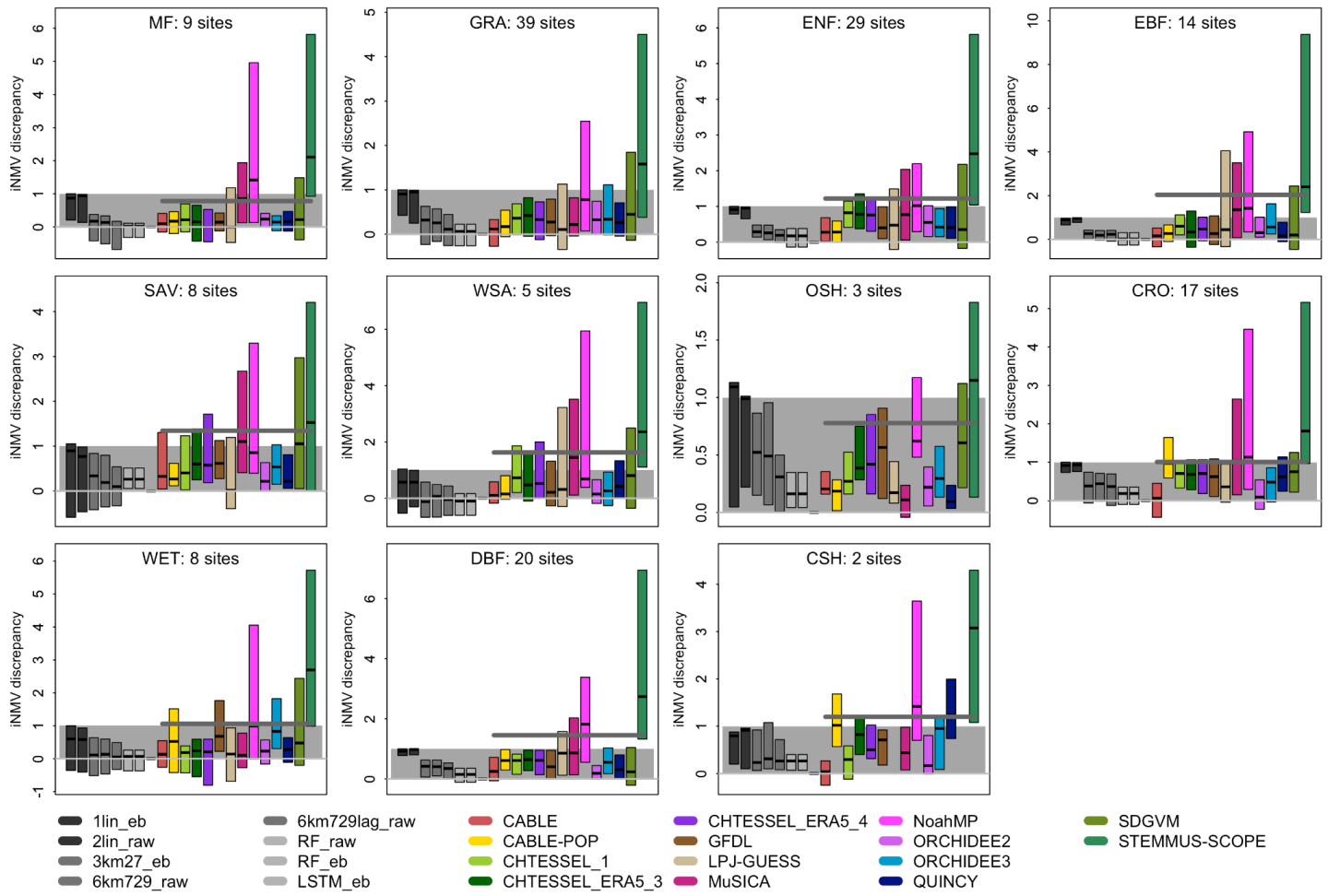
Figure S12d: Independent normalised metric value (iNMV) discrepancy between each model and LSTM_raw for net ecosystem exchange (NEE), sorted by vegetation type, as per Figure 7. Vegetation types are: Mixed Forest (MF); Grassland (GRA); Evergreen Needleleaf (ENF); Evergreen Broadleaf (EBF); Savanna (SAV); Woody Savanna (WSA); Open Shrubland (OSH); Cropland (CRO); Wetland (WET); Deciduous Broadleaf (DBF); Closed Shrubland (CSH).
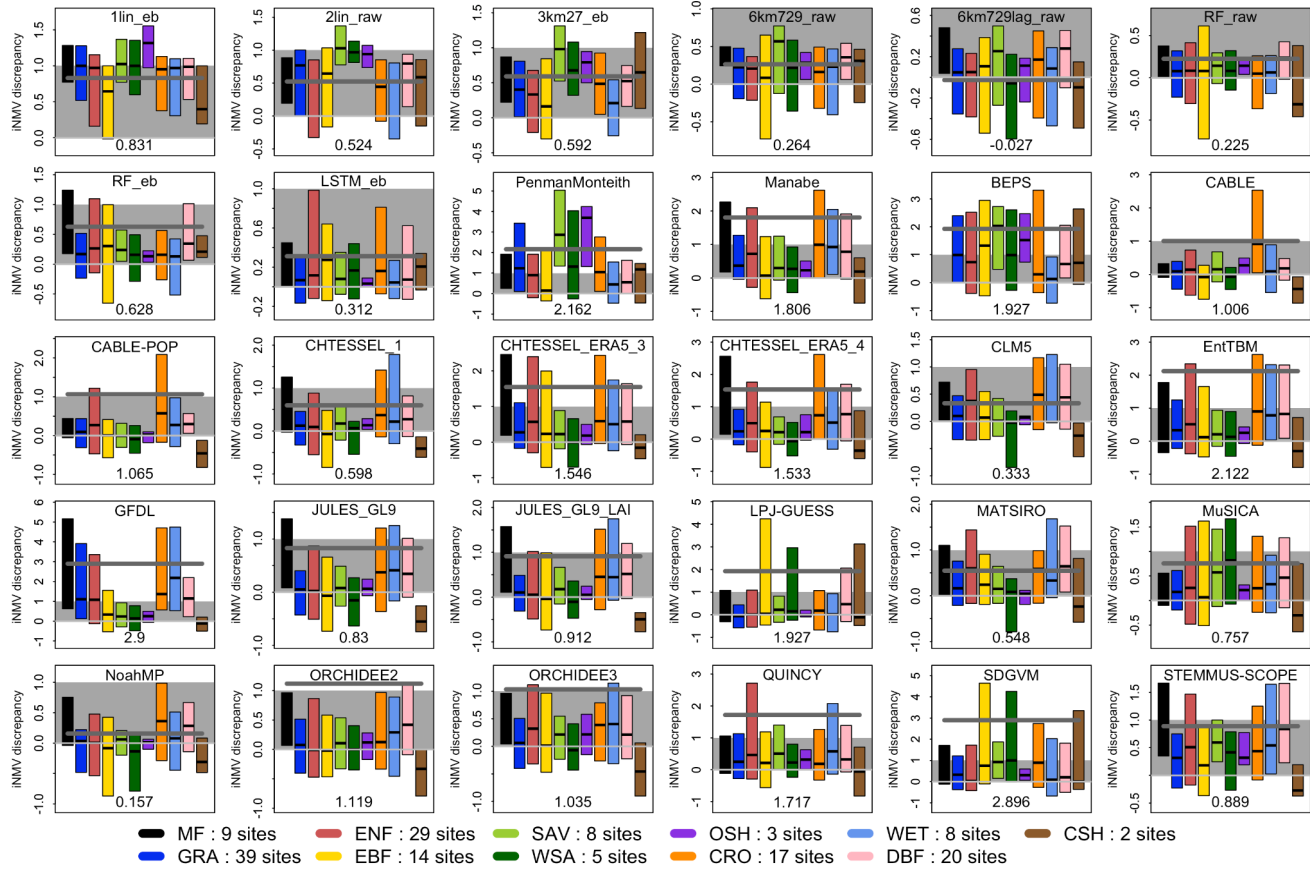
Figure S13a: Independent normalised metric value (iNMV) discrepancy between each mechanistic model and LSTM_raw for latent heat flux (Qle), with separate inter-quartile boxes for each vegetation type, using raw fluxes. Mean model discrepancy is shown by the dark grey line and text at the bottom of each panel, with reference empirical model range [0,1] shaded in grey. Vegetation types are: Mixed Forest (MF); Grassland (GRA); Evergreen Needleleaf (ENF); Evergreen Broadleaf (EBF); Savanna (SAV); Woody Savanna (WSA); Open Shrubland (OSH); Cropland (CRO); Wetland (WET); Deciduous Broadleaf (DBF); Closed Shrubland (CSH). Lower scores are better.
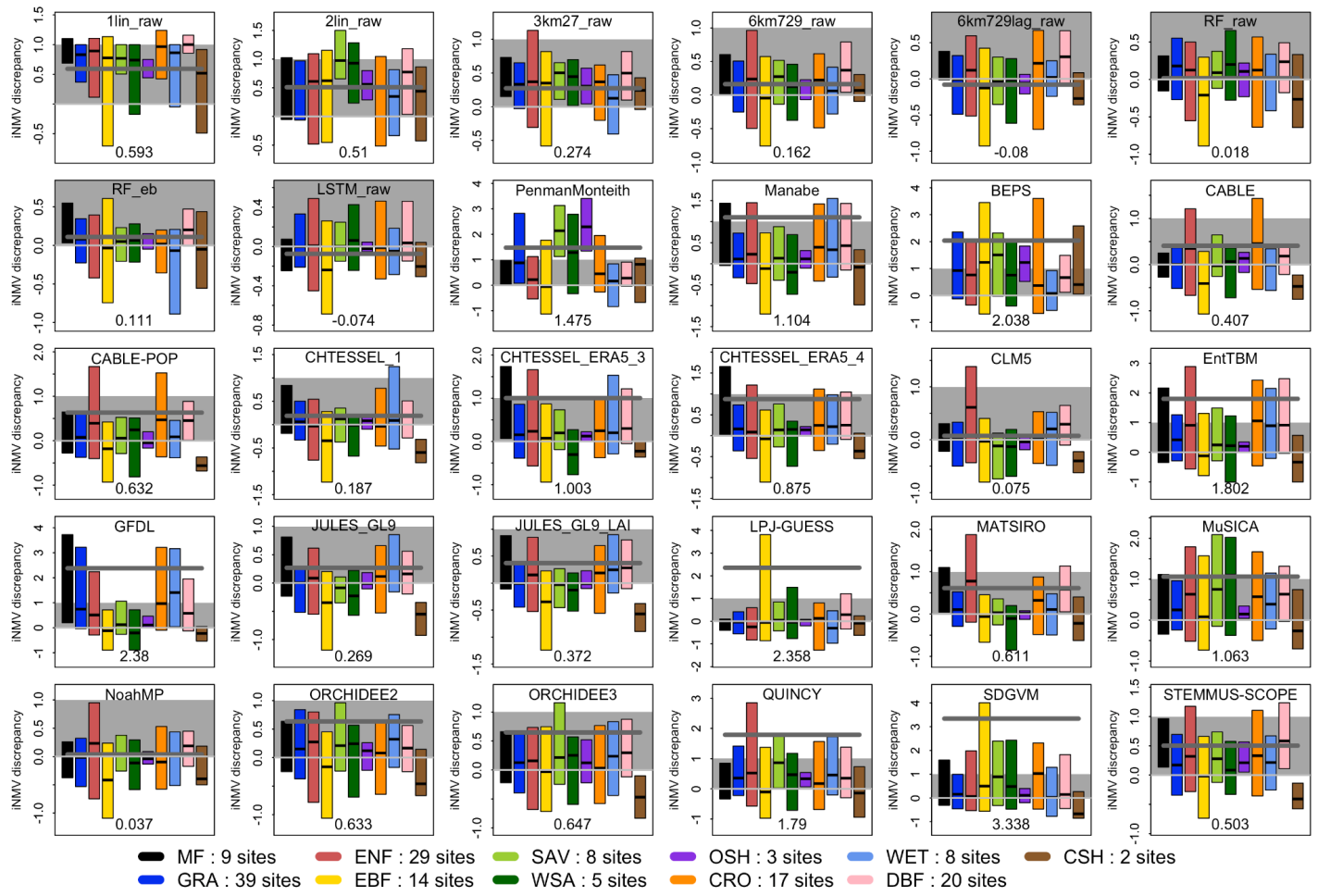
Figure S13b: Independent normalised metric value (iNMV) discrepancy between each mechanistic model and LSTM_eb for latent heat flux (Qle), with separate inter-quartile boxes for each vegetation type, using energy balance corrected fluxes. Mean model discrepancy is shown by the dark grey bar and text at the bottom of each panel, with 0-1 range (grey shading) representing the range of metric values between 1lin and LSTM_eb. Vegetation types are: Mixed Forest (MF); Grassland (GRA); Evergreen Needleleaf (ENF); Evergreen Broadleaf (EBF); Savanna (SAV); Woody Savanna (WSA); Open Shrubland (OSH); Cropland (CRO); Wetland (WET); Deciduous Broadleaf (DBF); Closed Shrubland (CSH).

Independent normalised metric improvement in Qh offered by LSTM_raw

Figure S13c: Independent normalised metric value (iNMV) discrepancy between each mechanistic model and LSTM_raw for sensible heat flux (Qh), with separate inter-quartile boxes for each vegetation type, using raw fluxes. Mean model discrepancy is shown by the dark grey bar and text at the bottom of each panel, with 0-1 range (grey shading) representing the range of metric values between 1lin and LSTM_raw. Vegetation types are: Mixed Forest (MF); Grassland (GRA); Evergreen Needleleaf (ENF); Evergreen Broadleaf (EBF); Savanna (SAV); Woody Savanna (WSA); Open Shrubland (OSH); Cropland (CRO); Wetland (WET); Deciduous Broadleaf (DBF); Closed Shrubland (CSH).
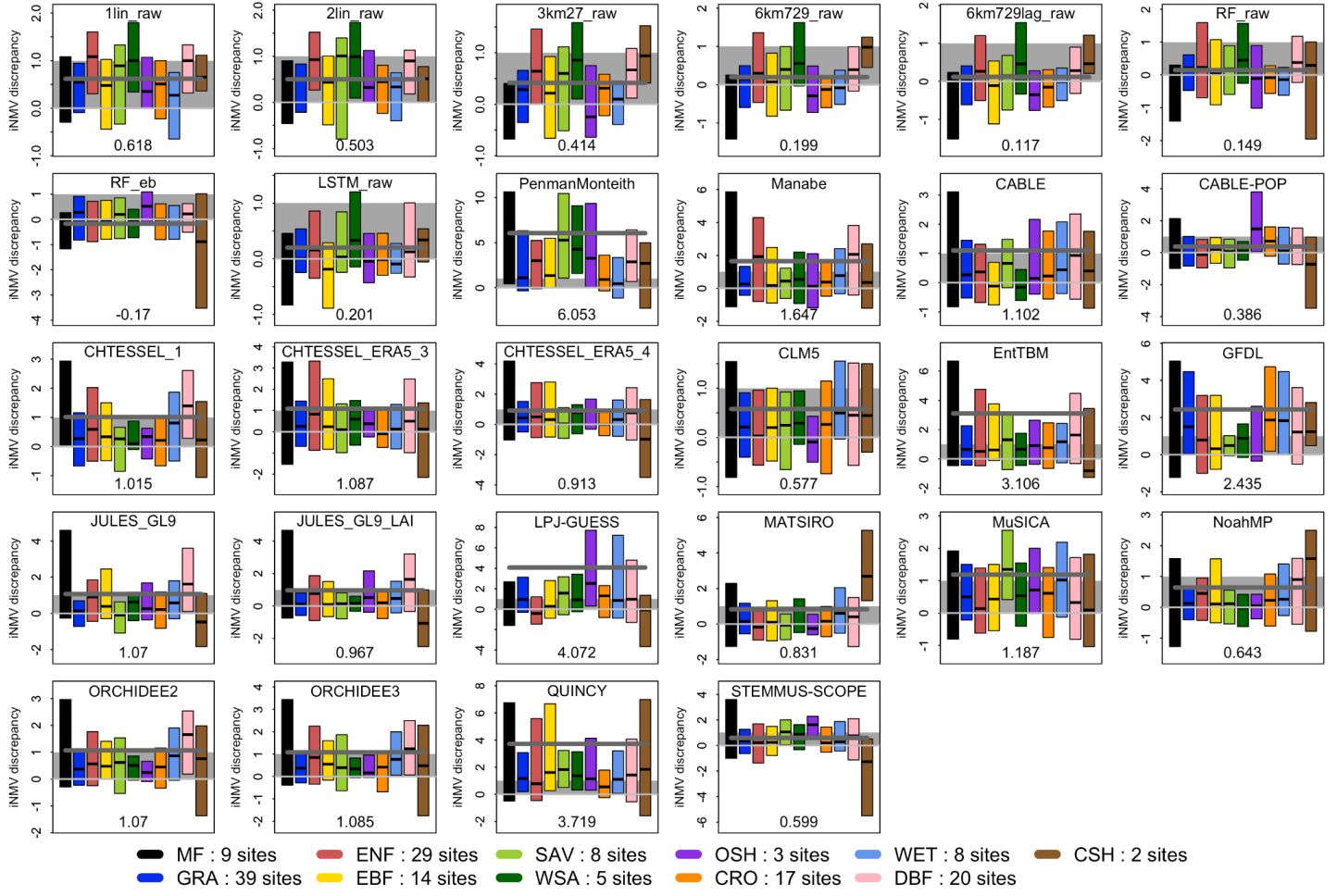
Figure S13d: Independent normalised metric value (iNMV) discrepancy between each mechanistic model and LSTM_eb for sensible heat flux (Qh), with separate inter-quartile boxes for each vegetation type, using energy balance corrected fluxes. Mean model discrepancy is shown by the dark grey bar and text at the bottom of each panel, with 0-1 range (grey shading) representing the range of metric values between 1lin and LSTM_eb. Vegetation types are: Mixed Forest (MF); Grassland (GRA); Evergreen Needleleaf (ENF); Evergreen Broadleaf (EBF); Savanna (SAV); Woody Savanna (WSA); Open Shrubland (OSH); Cropland (CRO); Wetland (WET); Deciduous Broadleaf (DBF); Closed Shrubland (CSH).

**Independent normalised metric improvement in NEE offered by LSTM_raw**

Legend:
MF : 9 sites, ENF : 29 sites, SAV : 8 sites, OSH : 3 sites, WET : 8 sites, CSH : 2 sites
GRA : 39 sites, EBF : 14 sites, WSA : 5 sites, CRO : 17 sites, DBF : 20 sites
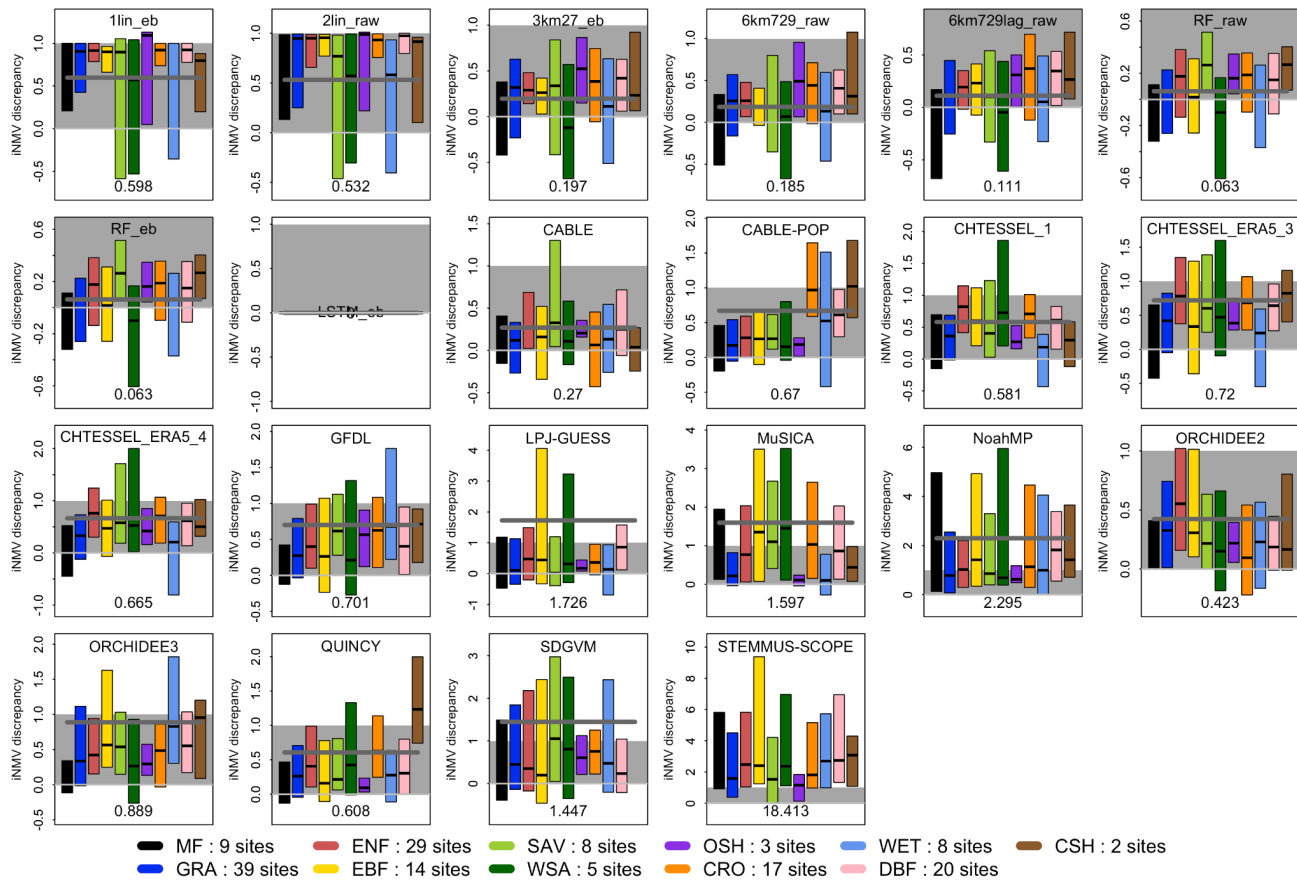
Figure S13e: As per Fig. 13a, but for Net Ecosystem Exchange of CO2 (NEE), for those LMs that reported NEE. Lower scores are better.
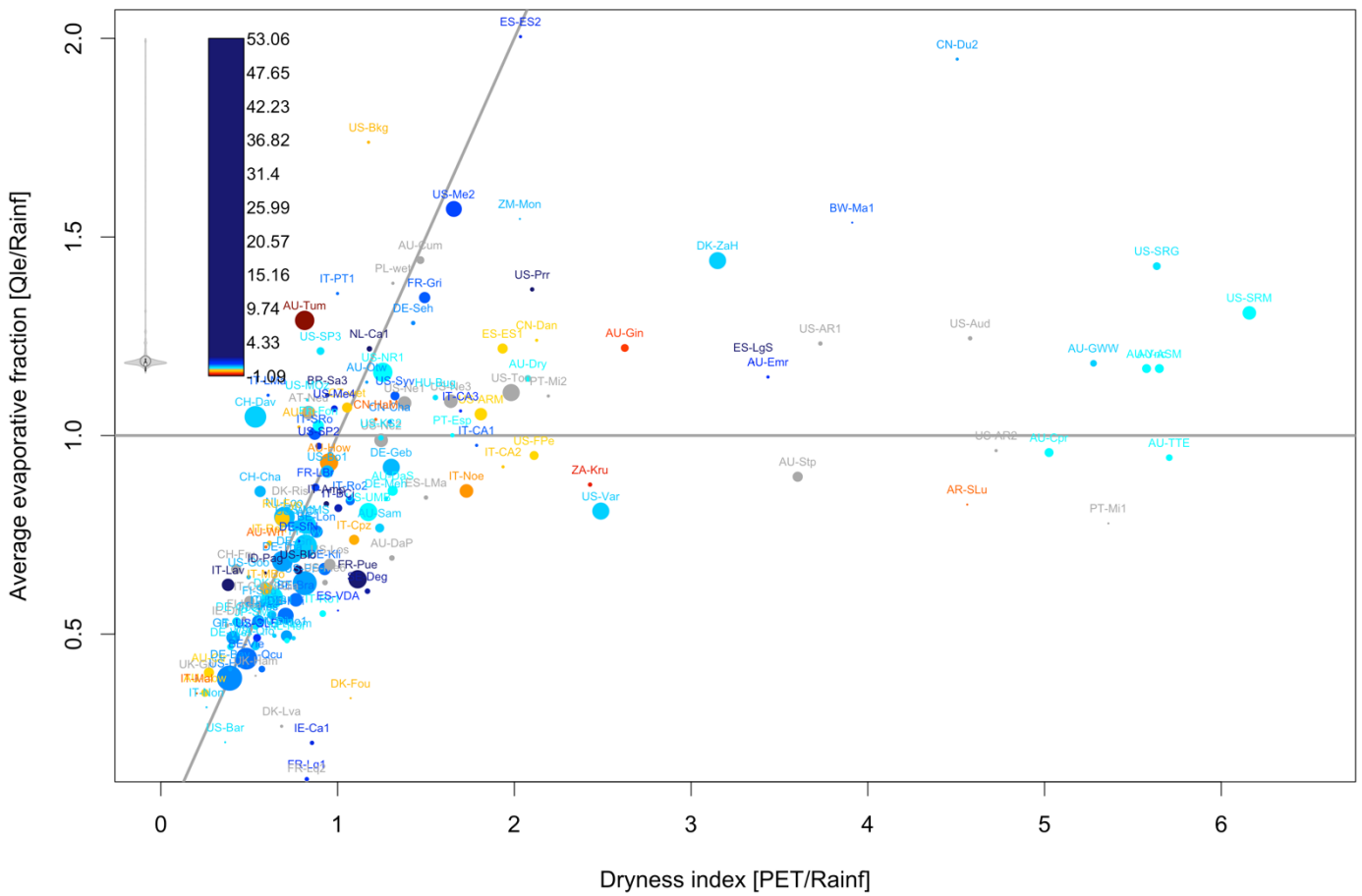
Figure S14a: Independent normalised metric value (iNMV) improvement offered by LSTM over the median iNMV value of all models, shown by colour for latent heat flux (Qle). Each site's location is shown on axes of observed evaporative fraction versus dryness index. The prevalence of particular colour values is shown by the violin plot to the left of the colour legend. Values within [-0.1,0.1] are shown in pink, and values above 2 have constant, dark blue colour. This is the same as Figure 8, but using energy-balance corrected Qle (which both changes the colour scale and location of sites on the graph). Dot sizes indicate the length of site data, ranging from 1 (smallest) to 21 years (largest) - see Table S2 for site details.
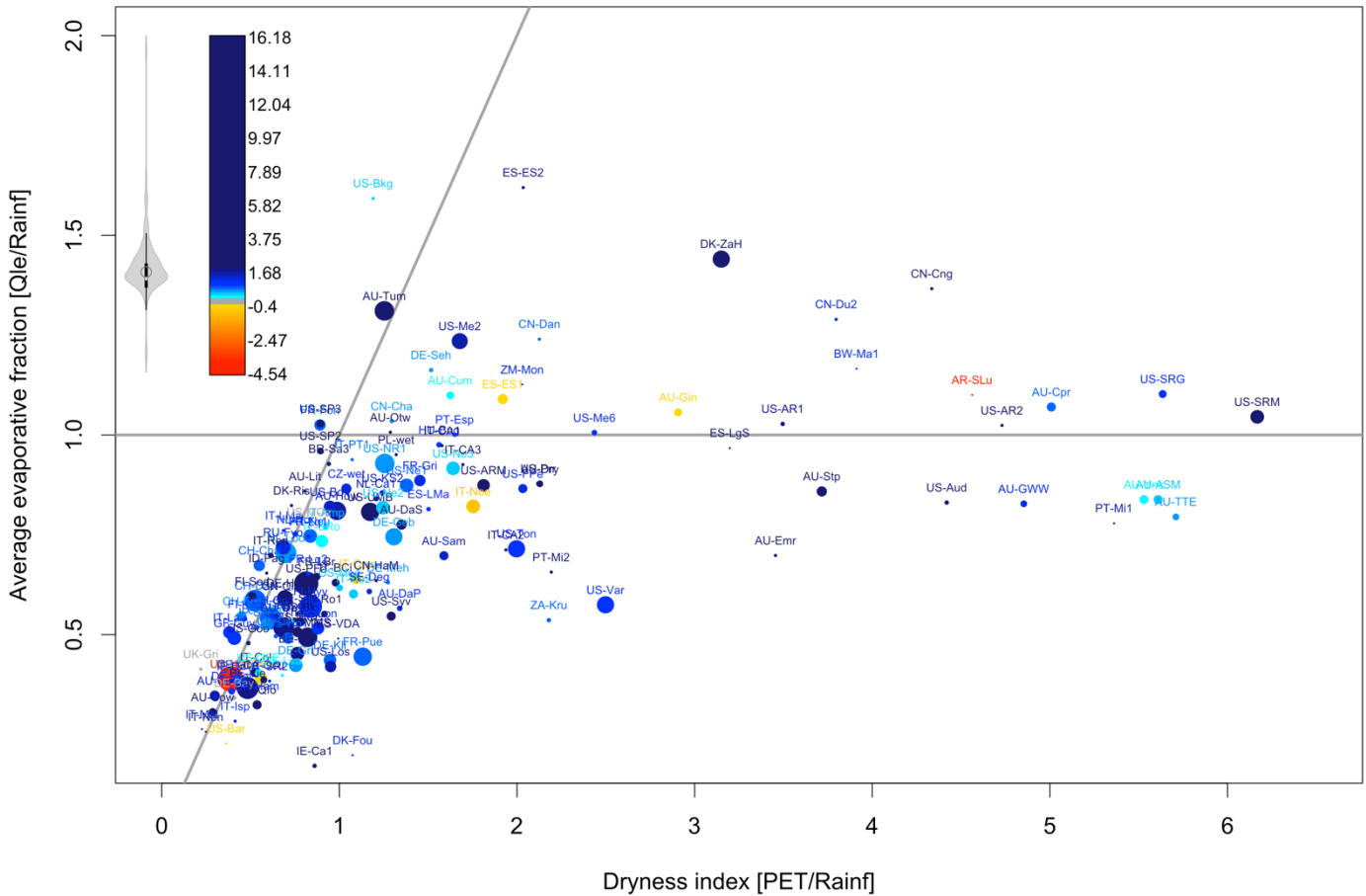
Figure S14b: Independent normalised metric value (iNMV) improvement offered by LSTM over the median iNMV value of all LMs (excluding empirical models), shown by colour for sensible heat flux (Qh). Each site's location is shown on axes of observed evaporative fraction versus dryness index. The prevalence of particular colour values is shown by the violin plot to the left of the colour legend. Values within [-0.1,0.1] are shown in pink, and values above 2 have constant, dark blue colour. Dot sizes indicate the length of site data, ranging from 1 (smallest) to 21 years (largest) - see Table S2 for site details.
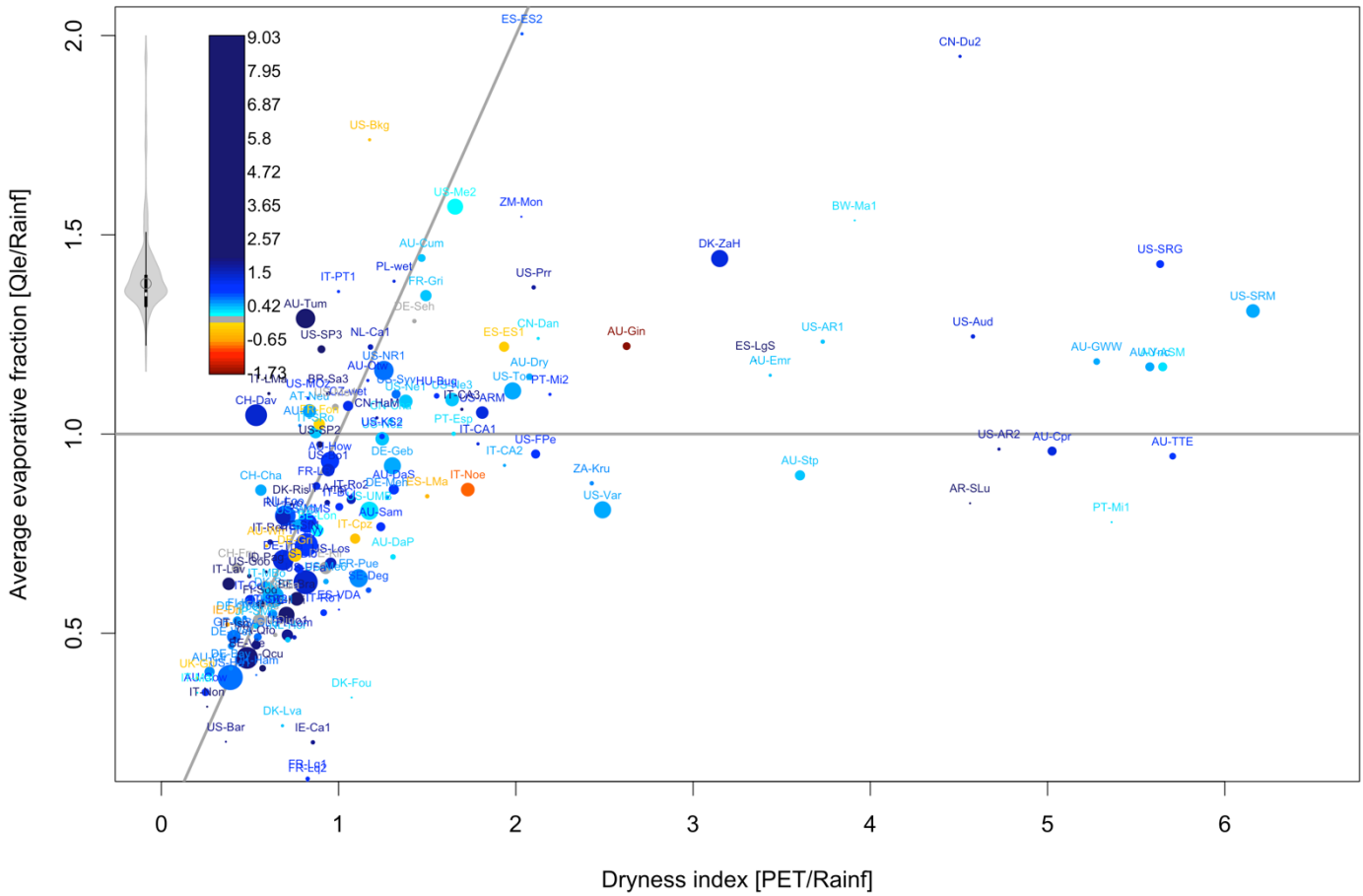
Figure S14c: Average normalised metric improvement offered by LSTM over each model in simulating sensible heat flux (Qh), averaged over all LMs (colour scale, excluding empirical models), with each site's location shown on axes of observed evaporative fraction versus dryness index. The prevalence of particular colour values is shown by the violin plot to the left of the colour legend. This is the same as Figure S14b, but using energy-balance corrected Qh (which changes the colour scale) and Qle (which changes location of sites on the graph). Dot sizes indicate the length of site data, ranging from 1 (smallest) to 21 years (largest) - see Table S2 for site details.
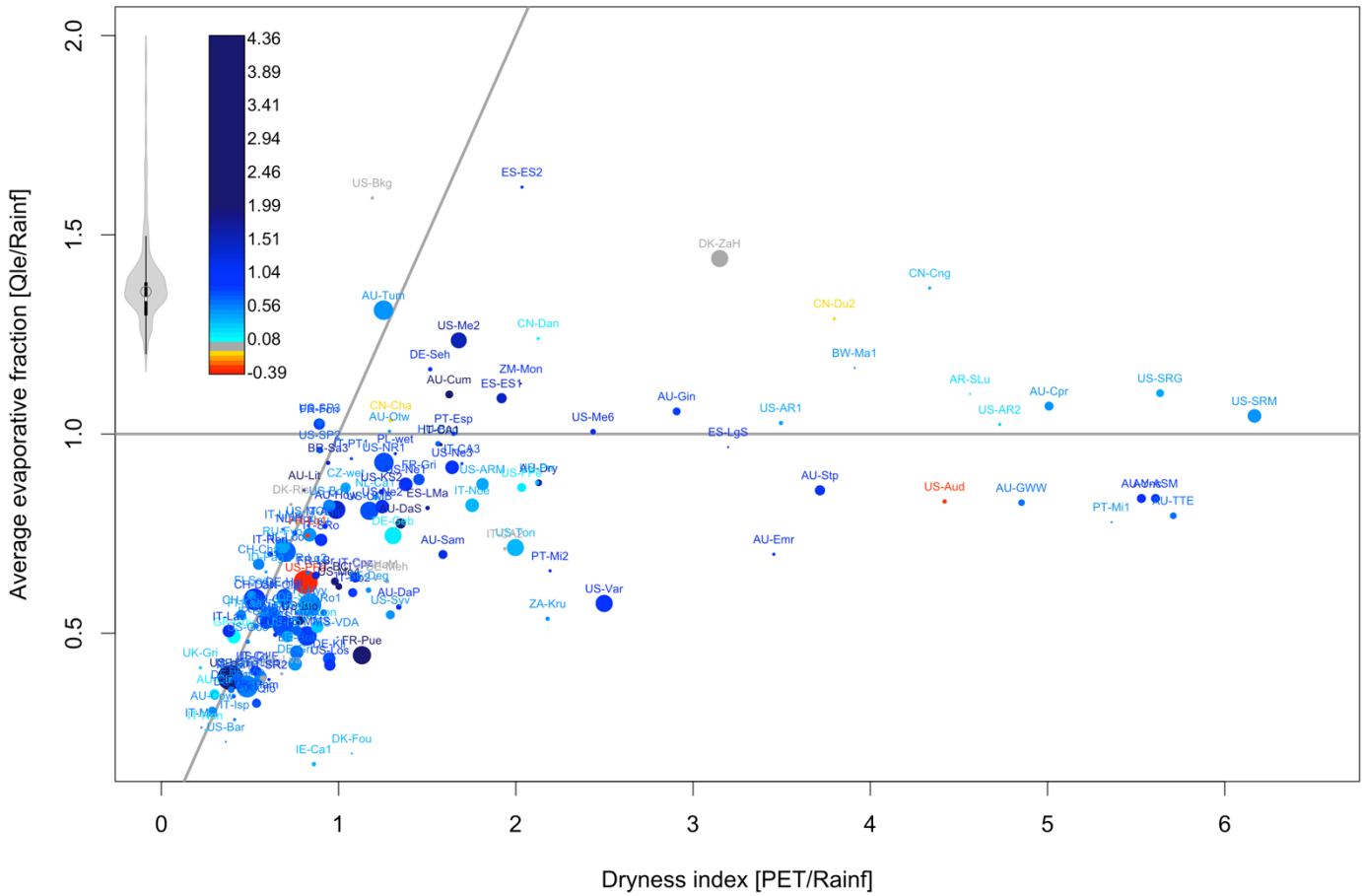
Figure S14d: Independent normalised metric value (iNMV) improvement offered by LSTM over the median iNMV value of all LMs (excluding empirical models), shown by colour for net ecosystem exchange (NEE). Each site's location is shown on axes of observed evaporative fraction versus dryness index. The prevalence of particular colour values is shown by the violin plot to the left of the colour legend. Values within [-0.1,0.1] are shown in pink, and values above 2 have constant, dark blue colour. Dot sizes indicate the length of site data, ranging from 1 (smallest) to 21 years (largest) - see Table S2 for site details.

References

Balsamo, G., Viterbo, P., Beljaars, A., van den Hurk, B., Hirschi, M., Betts, A. K., and Scipal, K.: A Revised Hydrology for the ECMWF Model: Verification from Field Site to Terrestrial Water Storage and Impact in the Integrated Forecast System, J. Hydrometeorol., 10, 623–643, https://doi.org/10.1175/2008JHM1068.1, 2009.

Best, M. J., Pryor, M., Clark, D. B., Rooney, G. G., Essery, R. L. H., Ménard, C. B., Edwards, J. M., Hendry, M. A., Porson, A., Gedney, N., Mercado, L. M., Sitch, S., Blyth, E., Boucher, O., Cox, P. M., Grimmond, C. S. B., and Harding, R. J.: The Joint UK Land Environment Simulator (JULES), model description – Part 1: Energy and water fluxes, Geosci. Model Dev., 4, 677–699, https://doi.org/10.5194/gmd-4-677-2011, 2011.

Clark, D. B., Mercado, L. M., Sitch, S., Jones, C. D., Gedney, N., Best, M. J., Pryor, M., Rooney, G. G., Essery, R. L. H., Blyth, E., Boucher, O., Harding, R. J., Huntingford, C., and Cox, P. M.: The Joint UK Land Environment Simulator (JULES), model description – Part 2: Carbon fluxes and vegetation dynamics, Geosci. Model Dev., 4, 701–722, https://doi.org/10.5194/gmd-4-701-2011, 2011.

Dunne, J. P., Horowitz, L. W., Adcroft, A. J., Ginoux, P., Held, I. M., John, J. G., Krasting, J. P., Malyshev, S., Naik, V., Paulot, F., Shevliakova, E., Stock, C. A., Zadeh, N., Balaji, V., Blanton, C., Dunne, K. A., Dupuis, C., Durachta, J., Dussin, R., Gauthier, P. P. G., Griffies, S. M., Guo, H., Hallberg, R. W., Harrison, M., He, J., Hurlin, W., McHugh, C., Menzel, R., Milly, P. C. D., Nikonov, S., Paynter, D. J., Ploshay, J., Radhakrishnan, A., Rand, K., Reichl, B. G., Robinson, T., Schwarzkopf, D. M., Sentman, L. T., Underwood, S., Vahlenkamp, H. , Winton, M., Wittenberg, A. T., Wyman, B., Zeng, Y., Zhao, M.: The GFDL Earth System Model Version 4.1 (GFDL-ESM 4.1): Overall coupled model description and simulation characteristics. J. Adv. Model Earth Syst., 12, e2019MS002015. https://doi.org/10.1029/2019MS002015, 2020.

Dutra, E., Balsamo, G., Viterbo, P., Miranda, P. M. A., Beljaars, A., Schär, C., and Elder, K.: An improved snow scheme for the ECMWF land surface model: description and offline validation, J. Hydrometeorol., 11, 899–916, https://doi.org/10.1175/2010JHM1249.1, 2010.

Gennaretti, F., Ogee, J., Sainte-Marie, J. and Cuntz, M.: Mining ecophysiological responses of European beech ecosystems to drought, Agr. Forest Meteorol., 280, 107780, doi: 10.1016/j.agrformet.2019.107780, 2020.

Haverd, V., Smith, B., Cook, G., Briggs, P., Nieradzik, L., Roxburgh, S., Liedloff, A., Meyer, C., and Canadell, J.: A stand-alone tree demography and landscape structure module for Earth system models. Geophys. Res. Lett., 40(19), 5234-5239. https://doi.org/10.1002/grl.50972, 2013.

Haverd, V., Cuntz, M., Nieradzik, L. P., and Harman, I. N.: Improved representations of coupled soil–canopy processes in the CABLE land surface model (Subversion revision 3432), Geosci. Model Dev., 9, 3111–3122, https://doi.org/10.5194/gmd-9-3111-2016, 2016.

Haverd, V., Smith, B., Nieradzik, L., Briggs, P. R., Woodgate, W., Trudinger, C. M., Canadell, J. G., and Cuntz, M.: A new version of the CABLE land surface model (Subversion revision r4601) incorporating land use and land cover change, woody vegetation demography, and a novel optimisation-based approach to plant coordination of photosynthesis, Geosci. Model Dev., 11, 2995–3026, https://doi.org/10.5194/gmd-11-2995-2018, 2018.

He, C., Valayamkunnath, P., Barlage, M., Chen, F., Gochis, D., Cabell, R., Schneider, T., Rasmussen, R., Niu, G.-Y., Yang, Z.-L., Niyogi, D., and Ek, M.: Modernizing the open-source community Noah with multi-parameterization options (Noah-MP) land surface model (version 5.0) with enhanced modularity, interoperability, and applicability, Geosci. Model Dev., 16, 5131–5151, https://doi.org/10.5194/gmd-16-5131-2023, 2023.

Hengl, T., Mendes de Jesus, J., Heuvelink, G. B. M., Ruiperez Gonzalez, M., Kilibarda, M., Blagotić, A., Shangguan, W., Wright, M. N., Geng, X., Bauer-Marschallinger, B., Guevara, M. A., Vargas, R., MacMillan, R. A., Batjes, N. H., Leenaars, J. G. B., Ribeiro, E., Wheeler, I., Mantel, S., and Kempen, B.: SoilGrids250m: Global gridded soil information based on machine learning, PLoS ONE, 12, e0169748, https://doi.org/10.1371/journal.pone.0169748, 2017.

Kim, Y., P.R. Moorcroft, I. Aleinov, M.J. Puma, and N.Y. Kiang : Variability of phenology and fluxes of water and carbon with observed and simulated soil moisture in the Ent Terrestrial Biosphere Model (Ent TBM version 1.0.1.0.0). Geosci. Model Dev., doi:10.5194/gmd-8-3837-2015, 2015.

Kowalczyk, E. A., Y. P. Wang, R. M. Law, H. L. Davies, J. L. McGregor, and G. S. Abramowitz, The CSIRO Atmosphere Biosphere Land Exchange (CABLE) model for use in climate models and as an offline model. CSIRO Marine and Atmospheric Research Paper 013, 43 pp., https://doi.org/10.4225/08/58615c6a9a51d, 2006.

Krinner, G., Viovy, N., de Noblet-Ducoudré, N., Ogée, J., Polcher, J., Friedlingstein, P., Ciais, P., Sitch, S. and Prentice, I. C.: A dynamic global vegetation model for studies of the coupled atmosphere-biosphere system, Global Biogeochem. Cy., 19, GB1015, doi:10.1029/2003GB002199, 2005.

Kumar, S. V., Peters-Lidard, C. D., Tian, Y., Houser, P. R., Geiger, J., Olden, S., Lighty, L., Eastman, J. L., Doty, B., Dirmeyer, P., Adams, J., Mitchell, K., Wood, E. F. and Sheffield, J.: Land information system: An interoperable framework for high resolution land surface modeling. Environ. Modell. Software, 21, 1402–1415, https://doi.org/10.1016/j.envsoft.2005.07.004, 2006.

Liu, J., Chen, J. M., Cihlar, J., Park, W. M.: A process-based boreal ecosystem productivity simulator using remote sensing inputs, Remote Sens. Environ., Volume 62, Issue 2, Pages 158-175, ISSN 0034-4257, https://doi.org/10.1016/S0034-4257(97)00089-8, 1997.

MATSIRO6 Document Writing Team, Description of MATSIRO6, CCSR Re- port No. 66, Division of Climate System Research, Atmosphere and Ocean Research Institute, The University of Tokyo, https://doi.org/10.15083/0002000181, 2021.

Niu, G.-Y., Yang, Z.-L., Mitchell, K. E., Chen, F., Ek, M. B., Barlage, M., Kumar, A., Manning, K., Niyogi, D., Rosero, E., Tewari, M., Xia, Y.: The community Noah land surface model with multiparameterization options (Noah-MP): 1. Model description and evaluation with local-scale measurements. J. Geophys. Res., 116, D12109, doi: 10.1029/2010JD015139, 2011.

Ogée, J., Brunet, Y., Loustau, D., Berbigier, P., and Delzon, S.: MuSICA, a CO_2, water and energy multilayer, multileaf pine forest model: evaluation from hourly to yearly time scales and sensitivity analysis, Glob. Change Biol., 9, 697–717, doi:10.1046/j.1365-2486.2003.00628.x, 2003.

Smith, B., Wårlind, D., Arneth, A., Hickler, T., Leadley, P., Siltberg, J., and Zaehle, S.: Implications of incorporating N cycling and N limitations on primary production in an individual-based dynamic vegetation model, Biogeosci., 11, 2027–2054, https://doi.org/10.5194/bg- 11-2027-2014, 2014.

Thum, T., Caldararu, S., Engel, J., Kern, M., Pallandt, M., Schnur, R., Yu, L., and Zaehle, S.: A new model of the coupled carbon, nitrogen, and phosphorus cycles in the terrestrial biosphere (QUINCY v1.0; revision 1996), Geosci. Model Dev., 12, 4781–4802, https://doi.org/10.5194/gmd-12-4781-2019, 2019.

van den Hurk, B. J. J. M., Viterbo, P., Beljaars, A. C. M., and Betts, A. K.: Offline validation of the ERA-40 surface scheme. ECMWF Tech. Memo. No. 295, 2000.

Walker, A. P., Quaife, T., van Bodegom, P. M., De Kauwe, M. G., Keenan, T. F., Joiner, J., Lomas, M. R., MacBean, N., Xu, C. G., Yang, X., J., and Woodward, F. I.: The impact of alternative trait-scaling hypotheses for the maximum photosynthetic carboxylation rate (V-cmax) on global gross primary production, New Phytol., 215, 1370–1386, 2017.

Wang, Y. P., Kowalczyk, E., Leuning, R., Abramowitz, G., Raupach, M. R., Pak, B., van Gorsel, E. and Luhar, A.: Diagnosing errors in a land surface model (CABLE) in the time and frequency domains. J. Geophys. Res., 116, G01034, doi:10.1029/2010JG001385, 2011.

Wang, Y., Zeng, Y., Yu, L., Yang, P., Van der Tol, C., Yu, Q., Lü, X., Cai, H., and Su, Z.: Integrated modeling of canopy photosynthesis, fluorescence, and the transfer of energy, mass, and momentum in the soil–plant–atmosphere continuum (STEMMUS–SCOPE v1.0.0), Geosci. Model Dev., 14, 1379–1407, https://doi.org/10.5194/gmd-14-1379-2021, 2021.

Woodward, F.I., Smith, T. M., and Emanuel, W.R.: A global land primary productivity and phytogeography model, Global Biogeochem. Cy., 9, 471– 490, https://doi.org/10.1029/95GB02432, 1995.

Woodward, F.I., and Lomas, M. R.: Vegetation dynamics – simulating responses to climatic change, Biol. Rev., 79, 643– 670, DOI: 10.1017/s1464793103006419, 2004.